CALCIUM - IRON WIRE INJECTION PRACTICE AT TISCO : THERMODYNAMIC MODELS AND INCLUSION ANALYSIS

A Thesis Submitted

in Partial Fulfillment of the Requirements

for the Degree of

Master of Technology

by

ANUP KUMAR

With compliments and respect to Dr. B. Deo

Anup Kumar

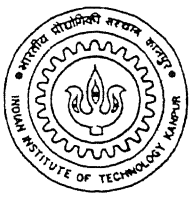

to the

DEPARTMENT OF MATERIALS AND METALLURGICAL ENGINEERING

INDIAN INSTITUTE OF TECHNOLOGY KANPUR

Brahma Deo 29.4.99.

Professor Brahma Deo
HEAD
Department of Materials & Metallurgical Engineering
Indian Institute of Technology
Kanpur-208 016, India

Certificate

It is certified that the work contained in the thesis entitled " Calcium – Iron wire injection practice at TISCO: Thermodynamic models and inclusion analysis " by Anup kumar, has been carried out under my supervision and the work has not been submitted elsewhere for a degree.

Brahma Deo 22.2.99.

Department of Materials and Metallurgical Engineering

Indian Institute of Technology

Kanpur 208016.

Feb, 1999

Dedicated to the memory of my father -
Late Anil Shanker Prasad, my mother -
Mrs. Shobha Prasad and my son Varun
Vishal.

Acknowledgment

I would like to express my heartfelt gratitude to, Prof. Brahma Deo, for his continuous encouragement, inspiration, support and valuable guidance during the course of my work. I would also like to express my gratitude to Prof. A.Ghosh, Prof. D. Mazumdar, Prof. R.Balasubramanium, Prof. P.K.Kalra and Prof. N. Chakraborty for teaching me various courses that I undertook in IIT Kanpur.

I would like to express my heartfelt gratitude to the management of The Tata Iron and Steel Co. Ltd., Jamshedpur for providing me a unique opportunity to pursue higher studies. It is my privilege to be associated with a company, which provides such unique opportunities to its employees for their academic improvement.

My special thanks are due to the members of our cricket team (Manish Pande, Vivek Mudgil, Ajay Gupta, Punyasheel and many others) for making my stay in IIT so interesting and active. My thanks are also due to Priyanka Sahay, Mrs. Bindu Gupta, Mrs. Nalini Mudgil and Mrs. Chhavi Pande.

My thanks are due to, Mr. A.J.Khan (TISCO), who helped me so much with the S.E.M. analysis of numerous samples.

Last but not the least, I am grateful to my wife (Mrs. Anupma kumar) who not only inspired me to pursue higher studies but also stood by me in difficult times.

List of Symbols:

P_{Ca}	: Vapour pressure of calcium.
P_0	: Atmospheric pressure.
ρ	: Density of liquid steel.
e^i_j	: Interaction parameter of 'i' on 'j'.
K	: Equilibrium constant.
$k^{'}$	: Apparent equilibrium constant.
[A] or, $\underline{A}$	: Dissolved concentration of element A in liquid iron.
[ ]	: Serial number (of list in the Reference Table) of the published literaure referred to.
$\Sigma_i (A_i)$	: $A_1 + A_2 + \ldots\ldots + A_n$

List of Tables:

	Page #
TABLE 1.1: Details of chemical composition of EWR and EWNR Steels	3
TABLE 1.2: Chemical composition and other details of Ca – alloy wire used in injection	3
TABLE 2.1: Compilation of equilibrium constants and interaction Parameters(at 1873 K)	20
TABLE 2.2: Activity values for individual equilibrium [8] reactions	20
TABLE 4.1: Inclusion area fraction in ladle and tundish samples	58
TABLE 4.2: Equilibrium constants and interaction parameters used in the thermodynamic model	59
TABLE 4.3: Slag activity data (1873 K)	60
TABLE 4.4: Comparison of calculated metal analysis by thermodynamic model	61
TABLE 4.5: O.L.P. chemical analysis (%) and temperature(°C)	62
TABLE 4.6: Actual chemical analysis of EWNR (mass %) steel	63
TABLE 4.7 a: Output of regression analysis with different chosen values of e_S^{Ca} (Slag activity: Rein and Chipman)	64
TABLE 4.7 b: Output of regression analysis with different chosen values of e_S^{Ca} (Slag activity : Ohto and Suito)	65
TABLE 4.8: Summarized output of linear regression	65

TABLE 4.9: Inclusion spot analysis result	66
TABLE 4.10a: List of G.A. inputs	67

List of Figures:

	Page #
Figure 1.1: Ellingham Diagram [1]	4
Figure 1.2: Process route for EWNR production followed at LD 1 – TATA STEEL	5
Figure 2.1: Influence of the molar concentration of Ca on the boiling point at various pressures [2]	21
Figure 2.2: Schematic diagram of T.N. Lance [3]	22
Figure 2.3: Schematic diagram of Wire Injection method	23
Figure 2.4: Schematic diagram of Wire lance method [4]	24
Figure 2.5: Comparison of calcium yield between Wire lance and Wire injection methods [4]	25
Figure 2.6: Vapour pressure of calcium as a function of temperature and the ferro-static head	26
Figure 2.7: $CaO - Al_2O_3$ binary phase diagram [7]	27
Figure 2.8: $CaO - Al_2O_3 - SiO_2$ ternary phase diagram at 1823K [9]	28
Figure 2.9: $CaO - Al_2O_3 - SiO_2$ iso-activity ternary diagram [10]	29
Figure 2.10:Influence of the lining materials on the change of [O] in iron after calcium addition [11]	30
Figure 2.11: Dissolved O_2 after aluminum deoxidation and hard argon Stirring [18]	31
Figure 2.12: Single phase modified inclusion [19]	32

Figure 2.13: Duplex $CaO-Al_2O_3$ inclusions with thin CaS layer [19]	33
Figure 2.14: $CaO- Al_2O_3$ inclusions with thick CaS layer [19]	34
Figure 2.15: CaS-MnS inclusion [19]	35
Figure 2.16: Complex calcium aluminate inclusion with Si and Mn [19]	36
Figure 2.17: Relationship of nozzle flow to increase in inclusion volume[20]	37
Figure 3.1 : Frequency distribution of dissolved oxygen at the end of Treatment	41
Figure 4.1: Frequency distribution of residual calcium in EWNR steels	68
Figure 4.2: Effect of slag carry over on calcium recovery	69
Figure 4.3: Typical $FeO - SiO_2$ inclusion observed in EWNR	70
Figure 4.4: Typical complex oxide inclusion observed in EWNR	71
Figure 4.5: Typical complex oxide inclusion with thin CaS layer	72
Figure 4.6: Typical complex oxide inclusion with thick CaS layer	73
Figure 4.7: Typical complex oxide inclusion with uniformly distributed Sulphur within the inclusion matrix	74
Figure 4.8: After injection treatment - slag composition plot	75

Figure 4.9 a: Iso-activity ternary diagram by Rein and Chipman [10]	76
Figure 4.9 b: Iso-activity ternary diagram by Ohto and Suito [27]	77
Figure 4.10: Plot between – log $_{10}$ k' and composition co-ordinate (z) [6]	78
Figure 4.11: Spot analysis of a typical inclusion found in H.No. 26785	79
Figure 4.12: Spot analysis of a typical inclusion found in H.No. 28503	80
Figure 4.13: Spot analysis of a typical inclusion found in H.No. 29530	81

ABSTRACT

Calcium – iron wire is injected in "Electrode Wire Non-Rimming (EWNR)" steel for reducing dissolved oxygen to obtain continuously cast billets free from pinholes and blowholes. Calcium – iron wire being expensive its consumption needs to be optimized.

In the beginning of the present study a detailed literature study has been carried out on various aspects of calcium injection viz. role of calcium in aluminum killed steels and its effect on the inclusion morphology, impact of process parameters on the efficiency of wire injection process etc.

Analysis of inclusions in steel samples carried out on "scanning electron microscope (S.E.M.)" has been presented next. This has been done with a view to find out the state of calcium retention in steel – whether dissolved or, completely associated with inclusions. S.E.M. analysis has revealed that the major part of the analyzed calcium (on optical spectroscope) is present as dissolved in liquid steel thus suggesting that there is a scope for optimizing the amount of calcium – iron in EWNR steel production at the Tata Iron and Steel Co. Ltd., Jamshedpur.

Existence of thermodynamic equilibrium between metal, slag and inclusion has been checked by using thermodynamic model and new values of interaction parameters and equilibrium constants have been estimated on the basis of data collected in the present work. Genetic adaptive search technique has been used to reestimate the values of interaction parameters and equilibrium constants.

Table of contents

Chapter 1. Introduction

1.1 Introduction 1
1.2 Scope of the present work 2

Chapter 2. Theoretical and Practical Aspects of Calcium Alloy Injection

2.1 Introduction 6
2.2 Methods of Injection of Calcium based Alloys in Steel Melt 6
2.3 Wire Injection Parameters 8
2.4 Thermodynamics of Ca-O Reaction 9
2.5 Influence of Ladle Refractory on the Rate and Degree of Deoxidation by Calcium Addition in Steel Making 12
2.6 Effect of Concentration of Dissolved Calcium on Inclusion Morphology, Composition and Amount 13
2.7 Mechanism of Calcium Sulphide Formation 13
2.8 Role of Calcium in Aluminum Killed Steel 14
2.9 Inclusion Modification in Calcium Treated Aluminum Killed Steel 15
2.10 Recovery of Calcium in Aluminum Killed Steel 16
2.11 Role of Calcium in Nozzle Blockage 18

Chapter 3. Injection Practice at TATA STEEL

3.1 Introduction 38
3.2 Specimen Preparation Procedure and SEM Examination Details 39

Chapter 4. Results and Discussions

4.1 Introduction 42
4.2 Scanning Electron Microscopic Observations of Samples 43
4.3 Assessment of Slag Metal Equilibrium on the Basis of Published Thermodynamic Data 44
4.3.1 Results of Thermodynamic model using published values of interaction parameters and equilibrium constants 46
4.4 Thermodynamic Model for the Simultaneous Determination of Interaction Parameters and Equilibrium Constants 48
4.4.1 Simultaneous Estimation of e^{Al}_{O} and $^{K}Al_2O_3$ on the basis of Aluminum- Oxygen equilibrium before wire injection 49
4.4.2 Thermodynamic Model for Simultaneous Estimation of e^{Ca}_{O}, e^{Ca}_{S} and ^{K}CaO 52
4.4.3 Thermodynamic Model for Simultaneous Estimation of e^{Al}_{O} and $^{K}Al_2O_3$ after wire injection 53

4.5 Application of Genetic Adaptive Search Technique to Evaluate Interaction Parameters and Equilibrium Constants 55

Chapter 5. Conclusions and Suggestions for Future Work

5.1 Conclusions 82
5.2 Suggestions for Future Work 83

References 84

Annexure 1 87

INTRODUCTION

Calcium injection in the form of wire or powdered alloys like Ca-Si, Ca-Fe, Ca-Si-Al is widely used in steel industry for obtaining low concentrations of dissolved oxygen (e.g. 2 - 3 ppm in Aluminum killed steel) as well as for inclusion modification. This is because calcium forms a very stable oxide (CaO) and sulphide (CaS) and lies towards the bottom of free energy - temperature diagram (Ellingham Diagram) [1] (see Figure1.1). At LD 1 plant of The Tata Iron and Steel Company (TATA STEEL), Ca-Fe wire injection is used in the production of Electrode Wire Non-Rimming (EWNR) steel. The typical Composition of EWNR is shown in Table 1.1.

Until a few years ago, the Electrode Wire grade (EWR) of steel, containing low levels of carbon, silicon (composition details are shown in Table 1.1), was produced at TATA STEEL through the rimming route. A major part of the EWR steel production has now been replaced by Electrode Wire Non Rimming steel. This is because the production of EWR steel requires a precise process control at each stage of operation, e.g. control of temperature at the tapping stage, controlled addition of rimming reagents to obtain gas evolution at the teeming stage, controlled addition of aluminum shots into the moulds in case of excessive rimming action during teeming and, finally, mechanical capping at the right time to terminate the rimming reaction. A slight error in anyone of the steps can spoil the material leading to low overall metal yield. In contrast with this, EWNR steel (process route shown in Figure 1.2) is processed through the continuous casting route. Continuous casting of EWNR steel also has posed the following problems:

(a) EWNR grade of steel has low concentrations of silicon and aluminum (Table 1.1). Therefore, billets are prone to pinholes and blowholes and the casting failures occur due to blockage of tundish nozzle.

(b) Complaints are received from wire rolling units regarding poor drawability (i.e. breakage of wire during rolling). Breakages occur due to the presence of hard inclusions. Scrappiness of the surface occurs due to reoxidation and poor deoxidation state of steel melt.

expensive and hence there is a need to optimize the consumption of Ca-Fe wire too.

1.2 Scope of the present work

The present work focuses on the theoretical and practical aspects of calcium based alloy injection into the liquid steel. Thermodynamic aspect (e.g. Ca and Al deoxidation) of EWNR steel have been studied by using operation data (metal analysis, temperature of liquid steel, slag analysis and dissolved oxygen readings) from plant and inclusion studies have been done on scanning electron microscope. The operation data have also been used to develop a mathematical model so as to extract the interaction parameters (e_S^{Ca}, e_O^{Ca}, e_O^{Al}) and equilibrium constants (K_{CaO}, K_{CaS}, K_{Al2O3}). Genetic adaptive search (GAS) technique is used as an alternative approach for the first time to reestimate the values of above mentioned interaction parameters and equilibrium constants.

Grade		C % (max)	Mn %	S % (max)	P % (max)	Si % (max)	Al % (max)	Ti % (max)
EWR	Specified Analysis	0.10	0.38 / 0.62	0.030	0.030	0.030	0.012	0.003
	Aimed Analysis	0.08	0.45 / 0.58	0.028	0.028	Trace	Trace	0.003
EWNR	Specified Analysis	0.10	0.38 / 0.62	0.025	0.025	0.030	0.012	0.003
	Aimed Analysis	0.06	0.40 / 0.55	0.020	0.020	0.028	0.012	0.003
	Actual Obtained Analysis *	0.05	0.49	0.015	0.021	0.027	<0.01	-

*Based on average product analysis of 35 heats.

TABLE 1.2: Chemical composition and other details of Ca – Alloy wire used in injection

	Ca – Fe (30/70)	Ca – Si (30/60)
Wire Diameter, mm	13	13
Wire Length/Spool, meter	3200	5000
Powder Weight (total), kg	923	1114
Ca in powder, %	30	30

TABLE 1.1: Details of chemical composition of EWR and EWNR steels.

Grade		C % (max)	Mn %	S % (max)	P % (max)	Si % (max)	Al % (max)	Ti % (max)
EWR	Specified Analysis	0.10	0.38 / 0.62	0.030	0.030	0.030	0.012	0.003
	Aimed Analysis	0.08	0.45 / 0.58	0.028	0.028	Trace	Trace	0.003
EWNR	Specified Analysis	0.10	0.38 / 0.62	0.025	0.025	0.030	0.012	0.003
	Aimed Analysis	0.06	0.40 / 0.55	0.020	0.020	0.028	0.012	0.003
	Actual Obtained Analysis *	0.05	0.49	0.015	0.021	0.027	<0.01	-

*Based on average product analysis of 35 heats.

TABLE 1.2: Chemical composition and other details of Ca – Alloy wire used in injection

	Ca – Fe (30/70)	Ca – Si (30/60)
Wire Diameter, mm	13	13
Wire Length/Spool, meter	3200	5000
Powder Weight (total), kg	923	1114
Ca in powder, %	30	30

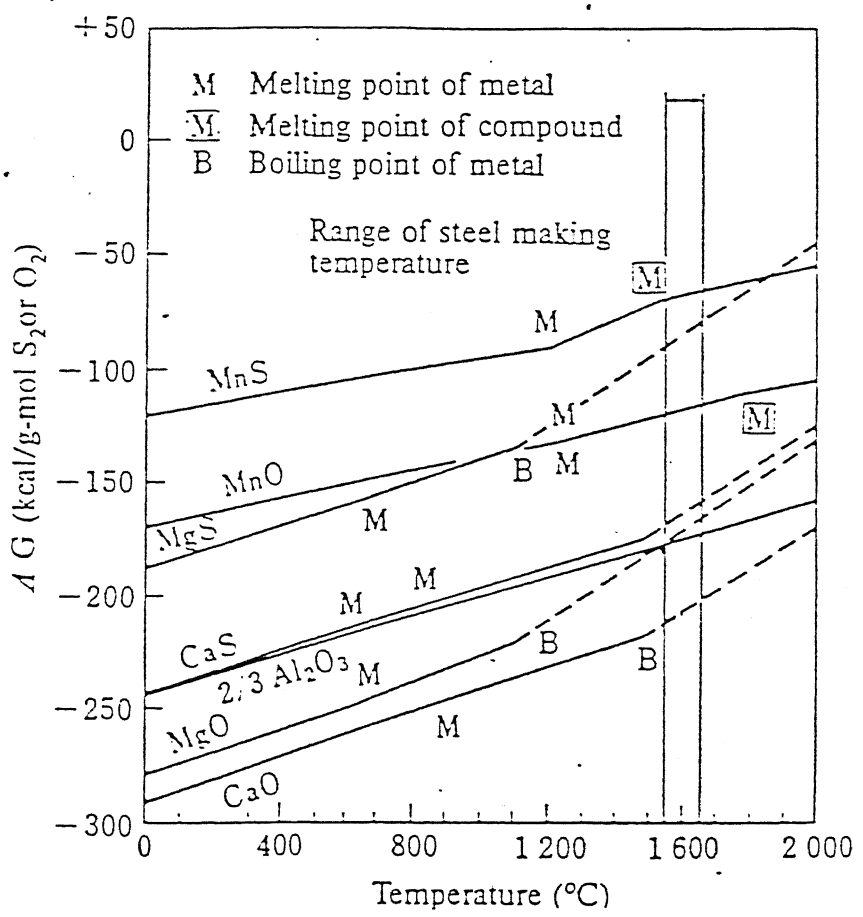

Figure 1.1: Ellingham Diagram

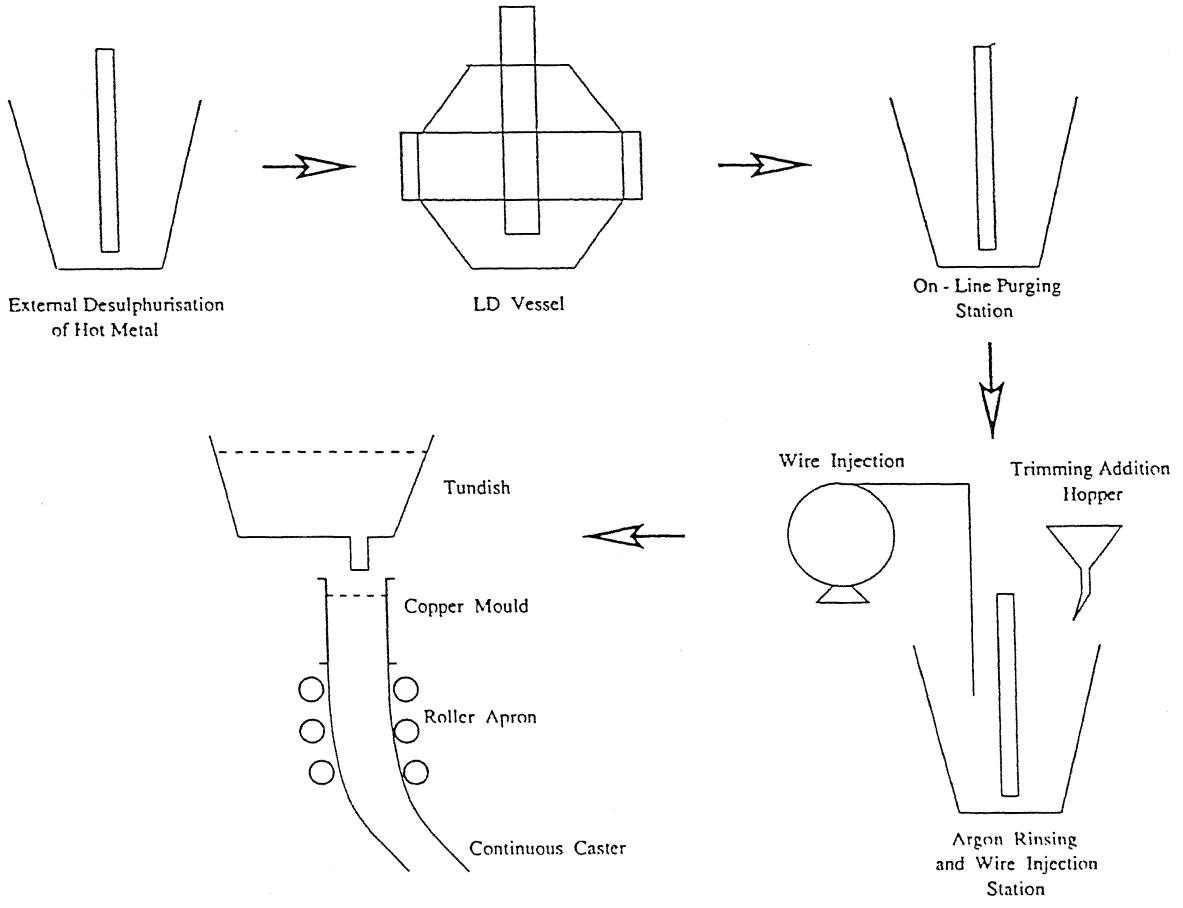

Figure 1.2: Process route for EWNR production followed at LD 1 – TATA STEEL.

CHAPTER 2

THEORETICAL AND PRACTICAL ASPECTS OF CALCIUM ALLOY INJECTION

2.1 Introduction

Practical aspects of calcium based alloy injection, including methods of injection and important injection parameters (such as treatment temperature, injection speed and the type of refractory) affecting the efficiency of wire injection process (such as calcium recovery, severity of blockage during casting operation) are first discussed along with the role of calcium in aluminum-killed steels and its effect on the inclusion morphology and composition. A review of the values of interaction parameters, equilibrium deoxidation constants (for Ca and Al) and desulphurisation constant (for Ca) as reported in literatures is also presented in this chapter.

2.2 Methods of Injection of Calcium Based Alloys in Steel Melt

The low melting point (approximately 850°C), low boiling point (approximately 1483°C) and high vapour pressure (2.2 - 3.7 atm. at 1600°C) of pure calcium necessitate special methods and procedures to be adopted for its injection into liquid steel. Owing to its high vapour pressure, addition of calcium in its pure metallic form is not recommended. Two or more component alloys containing Fe, Si and/or Al may be used. Figure 2.1[2] shows the effect of the molar concentration of Ca on the boiling point at various pressures for the three alloys, Ca - Al, Ca - Al - Si and Ca - Si. At a given temperature with decreasing calcium content, the boiling point of calcium increases and the vapour pressure decreases.

The popular methods of introducing calcium into the liquid steel are -

(i) ***Powder injection through a lance*** (TN Lance and Scandinavian Lance System): Powder injection through a lance system essentially comprises of a dispenser unit and a lance. In both the systems (schematic diagram shown in Fig

2.2) [3] powder is fluidized in the dispenser unit by using argon gas which also acts as carrier.

(ii) *Wire Injection*: The wire injection assembly (see Figure 2.3) comprises of a " pay off " on which Ca - alloy wire is loaded and the wire itself is pulled by a series of pinch rolls provided on the feeding machine. The wire enters the steel melt through a guide pipe. The wire contains steel sheath, which is tightly wrapped around a core of Ca and Fe powder (or CaSi etc.). When the wire enters the liquid steel, the outer steel sheath, being solid, withholds the release of low melting, low density and highly reactive core material. As the wire travels down in steel melt, surface temperature of the wire increases and the core materials melt and fuse with iron before getting released into the molten bath. This release at a location deep into the melt is necessary for a good recovery of calcium in melt.

The advantages of wire injection over the powder injection through a lance are:

- Wire injection is simpler and requires a lower level of technical expertise and supervision.
- The amount of liquid steel to be treated in lance injection must be large to reduce cost and heat loss per ton of steel and to increase recovery of calcium. The average yield of calcium ranges from 6 to 18 mass % for powder injection and 12 to 25 mass % for wire injection.
- The control of dissolved aluminum and temperature is superior in wire injection due to shorter treatment times and reduced metal - slag reaction (owing to lower argon flow rates needed during wire feeding).

In 1983 Pfizer Inc. [4] developed an injection process, termed as " ***Wire Lance Method*** ", which combines the features of both powder injection and the wire feeding method. In this method, as shown in Figure 2.4[4], calcium wire is fed into steel melt through a refractory lance which is submerged to approximately 2 meters below the liquid steel surface. Prior to feeding the wire, the lance is purged with an inert gas and the gas flow is maintained during the whole wire feeding operation.

Wire lance feeding has following advantages over the simple wire feeding method:

(a) The wire enters the melt at a depth determined by the lance immersion and therefore sufficient ferro-static pressure is provided to avoid boiling of the calcium at the location where the wire dissolves into the steel melt.

(b) Since, wire is protected by steel sheath, the calcium core reacts with the liquid steel only for about 1 second after the wire has entered the melt. Thus the calcium reaction takes place away from the lance tip and is not influenced by the gas bubbles coming out from the lance tip. Calcium vapour bubbles are created only when the calcium rises above the critical vaporization depth. As a result, bubbles are well dispersed in the melt. The dispersion of liquid calcium deep below the melt surface ensures a maximization of calcium - steel interaction. This increases calcium yield (see Figure 2.5) [4].

(c) In contrast with powder injection method, the inert gas has no carrier function and its flow rate can be adjusted solely for optimum stirring of the melt.

2.3 Wire Injection Parameters.

The ferro - static head created by the steel in the ladle is used to keep calcium in the liquid state while it dissolves and, modify the existing high melting temperature inclusions. The pressure head of liquid steel helps to suppress boiling point of calcium. For a given treatment temperature, the critical depth to which the wire must be injected (before it melts) to suppress calcium vaporization can be calculated as follows:

The vapour pressure of calcium for a given temperature is expressed by the following relationship:

$$\log_{10}P_{ca} = -8920/temp - 1.39\log_{10}(temp) + 12.45 \text{ [mm,Hg]} \qquad 2.1$$

The relationship between ferro - static head and depth of steel can be expressed by -

$$P = h \rho g + P_o \qquad 2.2$$

Where,

h = depth of liquid steel, m

ρ = density of liquid steel, kg/m^3 [7000]

g = acceleration due to gravity, m/sec^2 [9.8]

P_o = atmospheric pressure, atmosphere [1]

Now, from equation (2.1), at 1600°C

$$P_{ca} = P_o = 1376.4 \text{ mm Hg} = 1.81 \text{ atm}$$

And, from equation (2.2)

$$1.81 = 1.0 + h \rho g$$

or, $$h = 1.2 \text{ m}$$

The vapour pressure of calcium is plotted as a function of temperature and ferro-static pressure head of liquid steel in Figure 2.6.

Under normal conditions, it requires approximately 1 to 3 seconds for the steel clad metallic calcium wire to melt at steel making temperatures. Thus, if wire is fed at a speed of 150 m/min then the wire penetrates at least 2.5 meters into steel bath. Upon melting the globules of liquid calcium slowly float upwards, continuously reacting with the surrounding steel. The absence of gas phase provides a higher reaction time with the steel (owing to slower rising velocity of liquid vis a vis lighter gas bubbles). As soon as the unreacted calcium reaches the critical depth for boiling, a large vapour bubble forms which then rises rapidly to the surface. Oxidation of calcium at the melt surface produces a white smoke consisting mainly of oxide of calcium.

2.4 Thermodynamics of Ca-O Reaction

The deoxidation reaction for calcium is expressed as:

$$\underline{Ca} + \underline{O} \rightarrow CaO_{(s)} \qquad (2.3)$$

The equilibrium constant K_{Ca} of reaction (2.3) is defined in terms of (i) the apparent solubility product k'_{CaO} {defined as (mass % Ca × mass % O)} and (ii) the activity coefficient of component i, f_i (defined with respect to 1 mass % Henerian standard state):

$$\log_{10}(K_{Ca}) = \log_{10}(a_{CaO}) - \log_{10}(k'_{CaO}) - \log_{10}(f_{Ca}) - \log_{10}(f_O)$$

or,

$$\log_{10}(K_{Ca}) = \log_{10}(a_{CaO}) - \sum_j \{e_{Ca}^j \times (\text{mass } \% \text{ j})\} - \sum_i \{e_O^i \times (\text{mass } \% \text{ i})\} - \log_{10}(k'_{CaO})$$

Where, e_i^j is a first order interaction coefficient in a dilute system M-i-j and is defined as:

$$e_i^j = [\partial(\log_{10}(f_i) / \partial(\% j)]_{(i)(j)\to 0}$$

Several experimental studies on calcium deoxidation equilibrium have been reported but the apparent solubility product k'_{CaO} has been found to differ significantly, from one investigation to another (viz. values reported in [32] and [38] in Table 2.1 differ by a factor of 10^{-5}). Turkdogan [5] too has reported that the errors in the estimation of standard free energy of formation of CaO, as reported in literature, vary from 10 - 30 kJ/gm - mole.

The factors responsible for this error are:

- Difficulty in chemical analysis of dissolved oxygen and calcium at low concentrations
- Faulty E.M.F. measurements with oxygen sensor.

Thoria based solid electrolyte is generally used in the E.M.F. cell for measurements at low oxygen concentrations (2 - 5 ppm). It has been suggested that when thoria stabilized solid electrolyte probes are immersed for measurement of oxygen activity in the steel melt containing dissolved calcium, a chemical reaction may occur at the interface of melt and electrolyte:

$$ThO_2\,(s) + 2\,[Ca] = [Th] + 2\,CaO\,(s) \qquad (2.4)$$

$$[Th] / [Ca]^2 = 1.1\times10^{-7}$$

Since the metal does not contain thorium to start with, calcium reduces the thorium oxide at the electrolyte - melt interface. Thus there is a depletion of Ca in the immediate vicinity of the probe. The consequence of reaction (2.4) is that it causes a higher reading of oxygen activity in the vicinity of probe vis a vis bulk concentration of

Ca away from the electrolyte tip. Due to this problem, Gustafsson and Mellberg [6] have emphasized that the interaction parameters and equilibrium constants must be evaluated simultaneously.

The equilibrium deoxidation product during simultaneous deoxidation with calcium and aluminum may be either pure CaO, pure Al_2O_3, or calcium aluminate depending on the ratio of the activities of calcium and aluminum in the melt. As the ratio of the activity of calcium to the activity of aluminum increases (Figure 2.7)[7], the equilibrium deoxidation product shifts from alumina to calcia. Figure 2.7 also shows the melting points of the following phases:

Al_2O_3, $CaO.6Al_2O_3$, $CaO.2Al_2O_3$, $CaO.Al_2O_3$, $12CaO.7Al_2O_3$, $3CaO.Al_2O_3$ and CaO.

It may be noted that between the temperature range of 1823 K and 1923 K only $12CaO.7Al_2O_3$ phase is liquid. When steel is deoxidized with aluminum and calcium (i.e. Fe, Ca, O, and Al system), the activities of calcium and aluminum in two-phase regions (mentioned below) can be calculated by knowing the CaO and Al_2O_3 activities in these regions. Activity values of CaO and Al_2O_3 in CaO - Al_2O_3 system are summarized in Table 2.2 for the following phase equilibrium [8]:

$Al_2O_3(s)$ / $CaO.6Al_2O_3(s)$, $CaO.6Al_2O_3(s)$ / $CaO.2Al_2O_3(s)$, $CaO.2Al_2O_3(s)$ / $CaO.Al_2O_3(s)$, CaO. $Al_2O_3(s)$ / Liquid Phase, Liquid Phase / $3CaO.Al_2O_3(s)$ and $3CaO.Al_2O_3(s)$ / CaO (s).

The CaO - SiO_2 - Al_2O_3 ternary phase diagram is shown in Figure 2.8[9]. It can be seen that at 1823 K most of the region in the middle of ternary phase diagram is liquid. Since activities of CaO, Al_2O_3 and SiO_2 in the liquid region are known (Figure 2.9) [10], it is possible to calculate the corresponding activities / concentrations of dissolved silicon, aluminum and calcium in the liquid region.

2.5 Influence of Ladle Refractory on the Rate and Degree of Deoxidation by Calcium Addition in Steel Making

A comparative study [11], using three types of crucible materials - CaO, Al_2O_3 and MgO to find out the influence of type of refractory on the degree and rate of calcium deoxidation of steel melts (using 0.5 % Ca as Ca clad material) has shown that there is a linear decrease of oxygen with time and the final oxygen content is lowest for the Al_2O_3 crucible (Figure 2.10). For MgO crucible however, only a relatively small reduction in oxygen is observed. It is suggested that this difference in deoxidation power is a consequence of chemical affinity between deoxidation products and the crucible materials and also attack of crucibles by Ca at the temperatures of molten steel. For Al_2O_3 crucibles, Al will enter the melt (according to reaction 2.5), combine with oxygen (according to reaction 2.6) and thus contribute to the total deoxidation. On the other hand, in case of MgO crucibles, the Mg produced by the reaction 2.7 enters the melt in the form of vapour. The high vapour pressure (19 atm. at 1600°C) combined with low solubility of Mg in molten iron explains the low effect of Ca addition to an iron melt in a MgO crucible.

$$Al_2O_3 + 3\,Ca \rightarrow 2\,Al + 3\,CaO \qquad (2.5)$$

$$2Al + 3O \rightarrow Al_2O_3 \qquad (2.6)$$

$$MgO + Ca \rightarrow Mg(v) + CaO \qquad (2.7)$$

It is also observed that dissolved oxygen content decreases rapidly with in the first 10 sec. of Ca addition and then decreases at a much lower rate until a final constant value is reached. The Ca deoxidation process of an iron melt, stirred by high frequency heating, can be divided into three distinct stages:

Stage I: With in the first 10 sec. of Ca addition.

Stage II: Between 10 sec. until a constant [O] level is obtained and,

Stage III: Which represents the final equilibrium condition.

2.6 Effect of Concentration of Dissolved Calcium on Inclusion Morphology, Composition and Amount

It has been reported [12] that the solubility of calcium in low alloy steel is of the order of 165 ppm (at 1600°C and one bar pressure of calcium vapour). It is necessary to control the amount of dissolved calcium in liquid steel for several reasons:

(i) It affects steel cleanliness due to modification of alumina clusters into small, globular calcium alumino silicates.

(ii) It improves steel fluidity due to transformation of high melting alumina silicates into low melting calcium alumino silicates.

(iii) It affects machinability due to transformation of hard alumina particles into soft calcium alumino silicates.

(iv) It prevents formation of harmful manganese - sulphide stringers by modification of sulphide inclusions. Enhanced plasticity of manganese - sulphide - calcium - sulphide (Mns - CaS) has been found to be dependent on the content of calcium - sulphide. For products, which require a small reduction ratio during rolling, only a partial modification of MnS to MnS - CaS is needed. For the rolled products requiring a heavy reduction, MnS should be completely modified into small and hard calcium sulphides (CaS).

2.7 Mechanism of Calcium Sulphide Formation

The free energies of formation for CaO and CaS are -240.0 (kcal/mole) and -200.0 (kcal/mole) [1], respectively, at 1873 K and thus under normal conditions, since CaO is more stable than CaS, the latter does not precipitate directly from the steel melt. Prior killing of steel with Al is necessary so that CaS can become thermodynamically stable due to the reaction -

$$3\,CaO + [S] + 2\,[Al] = CaS + Al_2O_3$$

Following mechanisms of formation of CaS have been suggested [13 - 16]:

(1) Sulphur is absorbed by the (Ca,Al)O compounds. During solidification, the CaO - Al_2O_3 inclusions act as nuclei for the crystallization of the dissolved Ca and S either on the outside or, within the particles.

(2) Initially, single phase CaO - Al_2O_3 - CaS compounds with a homogeneous CaS content exists in the melt. During solidification the CaS precipitates because of the reduced solubility in CaO - Al_2O_3, a ring-shaped layer is attributed to the effects of the surface tension.

(3) Agglomeration of CaO - Al_2O_3 and CaS particles by diffusion and collision process.

(4) In case of a high Ca addition to the steel, the CaO content of the core and the CaS content of the outer layer may increase to an extent that the particle transforms into single phase $CaO.Al_2O_3$ - CaS compound.

2.8 Role of Calcium in Aluminum Killed Steel

When Calcium is injected into aluminum killed steel as Ca alloy (e.g. CaFe , CaAlFe, CaSi, CaAl etc.), a series of reactions may occur:

$$Ca(l) \rightarrow Ca(g)$$

$$Ca(g) \rightarrow [Ca]$$

$$[Ca] + [O] \rightarrow CaO$$

$$[Ca] + [S] \rightarrow CaS$$

$$[Ca] + (x + 1/3)Al_2O_3 \rightarrow CaO.xAl_2O_3 + 2/3[Al]$$

Depending on the steel composition as well as the manner of calcium injection and other process variables, solid alumina inclusions may transform to molten aluminate inclusions. The smaller inclusions will be converted to molten calcium aluminate more readily than the larger inclusions. Turkdogan [17] has shown that the calcium aluminate ladle slag enhances the extent of deoxidation with aluminum. In the plant trials with 30-ton AOD heats, Riley and Nusselt [18] took the oxygen readings with the help of oxygen sensors after vigorous argon stirring of steel with the lime aluminate slag. As seen from

the Figure 2.11, the residual oxygen contents at 1650°C and 1600°C are below the equilibrium curves for pure alumina. This is because of the fluxing of alumina inclusions with the calcium aluminate slag in the presence of stirring. A similar castability and cleanliness improvement in aluminum killed steels has been observed at various steel plants by employing either CaSi treatment or, stirring in presence of lime rich aluminate slag.

2.9 Inclusion Modification in Calcium Treated Aluminum Killed Steel

The morphology and the composition of the final inclusions depend on residual contents of Al, S and Ca in steel. For sulphur contents less than 0.010 mass %, calcium treatment produces essentially lime aluminate. For sulphur contents of the order of 0.015 mass % the calcium action on the sulphides is more effective. When the dissolved calcium, [Ca], is approx. 20 ppm the core of aluminates is associated with manganese sulphides, which are rich in calcium. For calcium content exceeding 30 ppm the sulphides of calcium surround the aluminates. The complex inclusions are round and do not deform much by hot deformation. At sulphur levels between 0.015 - 0.020 mass % the oxi - sulphides are predominant (aluminates with a sulphide sheath).

The inclusions formed during the Ca treatment have a substantially higher CaO content than the ones precipitated during the subsequent cooling from the residual dissolved oxygen or, during reoxidation (assuming that these new inclusions are not reacting with the high temperature ones). This is particularly true in medium to high sulphur steels (S > 0.03 %), in which part of the calcium is fixed as CaS (formed mostly during the calcium treatment). In extreme cases, however, some CaS can precipitate during the cooling.

Calcium action on alumina is strong in the beginning then it decreases and stabilizes. In the first 10 seconds of calcium treatment, big round shaped aluminates are formed with high calcium content (40 - 60 %) having low density and low melting point. Because of high superficial tension, these inclusions tend to agglomerate together and float up quickly if a gentle gas bubbling is applied over a long time. As a result of floatation, both the alumina content and the total oxygen content decrease. Presern [19] has

suggested that modified inclusions in calcium treated aluminum killed steels could be classified into five different types:

Type 1 (Single Phase Modified Inclusion): Figure 2.12 shows that sulphur is dissolved homogeneously in a single phased $CaO-Al_2O_3$ inclusion. High solubility of sulphur in $CaO-Al_2O_3$ system is the reason for such a type of inclusion. If the sulphur content is low enough, no precipitation occurs during cooling and sulphur remains dissolved and uniformly distributed in the inclusion.

Type 2 (Duplex $CaO-Al_2O_3$ inclusions with thin CaS layer (Figure 2.13): This is the most common form of a modified inclusion by proper calcium additions. In this case the steel contains modified liquid calcium aluminate with dissolved sulphur. During cooling and solidification of steel the solubility of sulphur diminishes and it starts to precipitate as CaS on the surface of modified calcium aluminate.

Type 3 ($CaO-Al_2O_3$ inclusions with thick CaS layer): such inclusions (Figure 2.14) decrease the castability of steel because they have a high melting point. It is suggested that formation of such inclusions is due to high contents of calcium and sulphur for a given aluminum content in the steel. The basic modification process of alumina inclusion is omitted due to the formation of thick CaS layer on the inclusion surface in the liquid steel.

Type 4 (CaS-MnS inclusion): Inclusion of CaS-MnS type (Figure 2.15) can be found in solidified steel in globular form only. They are formed during solidification when calcium reacts with MnS. It is reported that such inclusions do not elongate during rolling.

Type 5 (Complex Calcium Aluminate with Si and Mn): These inclusions (Figure 2.16) usually contain silicon and manganese.

2.10 Recovery of Calcium in Aluminum Killed Steel

In spite of a large number of studies on the deoxidizing power of various elements and the composition of deoxidation product, even today the recovery of deoxidiser elements and the type and distribution of the resultant inclusions are not fully predictable.

The metallurgical factors controlling the effectiveness and efficiency of calcium treatment are:

- Solubility of calcium in the steel.
- Oxygen content in the steel bath.
- Bath temperature.

- **Calcium Solubility**: On the basis of experimental work, Sponsoller [12] suggested that the limit of calcium dissolution in steel can be increased by increasing the concentrations of elements such as C, Si and Ni in steel. He also noted less metal splashing as the concentrations of these elements increase. Thus, a low calcium retention and violent reaction in the form of metal splashing is expected in low carbon steels during calcium injection treatment.

- **Oxygen Content of steel bath**: Lower oxygen content in the steel bath before calcium treatment allows higher calcium concentration in the finished steel. The slag should also be low in FeO to minimize both oxidation and calcium fade.

- **Bath Temperature**: Higher temperature allows greater amount of calcium to be in equilibrium with higher level of dissolved oxygen. Therefore, if higher calcium residuals are required in the finished steel, higher temperature need to be used. However, higher treatment temperatures promote gassification of the calcium, which results in lower calcium.

Gaye et al [20] showed that for a given final composition of the steel the higher the treatment temperature, higher is the CaO content of inclusion.

2.11 Role of Calcium in Nozzle Blockage

Clogging of ladle nozzle occurs when solid or partially solid inclusions are present in the steel and get deposited at the nozzle. In the case of Al-killed calcium treated steels, two different situations of blockage are to be considered. One of them takes place when calcium content in the steel flowing through the nozzle is too low to fully liquify Al_2O_3 inclusions generated during deoxidation. The other situation may occur when calcium content is too high (for a given S, Al and O content) such that solid CaS inclusions are produced. In addition to this it is also observed that, unless the calcium concentrations in steel exceeds a threshold value, there is an increase in the severity of nozzle blockage. This occurs when the major inclusion phase formed is $CaO.6Al_2O_3$ instead of Al_2O_3. The reasons for blockage are (a) the $CaO\ .6Al_2O_3$ phase is solid (melting point: 1830°C) at steel making temperatures (b) when $CaO.6Al_2O_3$ phase forms instead of Al_2O_3, the inclusion volume increases by 14 %. Faulring [21] reported that it is the volume of the solid inclusions formed that determines the severity of nozzle blockage and not the mass percent (see Figure 2.17).

Bhattacharya and Pielet [22] analyzed the non - metallic inclusions in plugged nozzle of calcium injected heats deoxidized with (i) only silicon and (ii) a simultaneous deoxidation with Silicon - Aluminum. Plugged nozzles in silicon killed heats showed solid calcium silicate together with calcium sulphide whereas, solid calcium sulphide was observed in silicon - aluminum killed heats.

Thermodynamic considerations have shown that the composition of oxide formed due to simultaneous deoxidation with silicon and calcium or with Al - Ca - Si is determined by the concentration and deoxidation power of each deoxidiser. Therefore, with calcium aluminum deoxidation a small amount of calcium in steel can cause a liquid calcium aluminate to form, while with calcium - aluminum - silicon deoxidation the same small amount of calcium can cause a solid calcium silicate to form.

Farrel & Hilty [23] studied the nozzle blockage in calcium treated aluminum killed steel and concluded the following:

All the deoxidants employed during steel making such as aluminum, silicon, zirconium, titanium, calcium etc. form oxide phases which are solid and refractory and

have low solubility in molten steel. Thus, unfloated deoxidation products or, reoxidation products of these elements precipitate and accumulate in the nozzle as a result of reduction in their solubility with falling temperature during casting. Their continued accumulation during the course of teeming ultimately results in complete blocking of the nozzle.

Various mechanical methods are suggested to combat blockage problem e.g. use of oversized nozzles, self-eroding nozzles, gas purging of nozzles, stopper rod control of tundish nozzles in strand casting. Maintaining the nozzles at a temperature equal to or above that of the molten steel, and preventing any temperature drop from taking place in the steel between furnace and mould during a cast should completely eliminate the blockage. A large-scale implementation of such ideas may pose serious equipment problems.

TABLE 2.1: Compilation of Equilibrium constants and Interaction parameters (at 1873 K)

k'_{CaO}	e_O^{Ca}	e_S^{Ca}	e_O^{Al}	$^{K}Al_2O_3$	k'_{CaS}
1×10^{-10} [32]	-310 [41]	-106 [34]	-1.17 [41]	2.7×10^{-13} [41]	1.7×10^{-5} [36]
2.5×10^{-9} [33]	-600 ± 80 [43]	-110 [39]	-4.21 [42]	1.6×10^{-14} [43]	6.3×10^{-8} [34]
5.5×10^{-9} [34]	-60 ± 4 [43]	-40 [40]	-5.25 [46]	1×10^{-13} [45]	3.7×10^{-7} [47]
4.5×10^{-8} [35]	-3600 [44]	-100 [41]	-12 [54]	5.6×10^{-14} [6]	2.1×10^{-9} [47]
9×10^{-7} [36]	-62 [6]	-178 [48]		2.4×10^{-14} [46]	6.3×10^{-4} [38]
1.6×10^{-6} [37]	-475 [34]			2.5×10^{-14} [49]	2×10^{-4} [52]
1.7×10^{-5} [38]	-535 [32]			3.8×10^{-12} [49]	2×10^{-7} [53]
7×10^{-8} [41]					

TABLE 2.2: Activity values for individual equilibrium

Equilibrium on the phase borders	^{a}CaO	$^{a}Al_2O_3$
CaO / Liquid	1.0	0.017
$12CaO.7Al_2O_3$	0.34	0.064
Liquid / $CaO.Al_2O_3$	0.15	0.275
$CaO.Al_2O_3$ / $CaO.2Al_2O_3$	0.10	0.414
$CaO.2Al_2O_3$ / $CaO.6Al_2O_3$	0.043	0.631
$CaO.6Al_2O_3$ / Al_2O_3	0.003	1.0

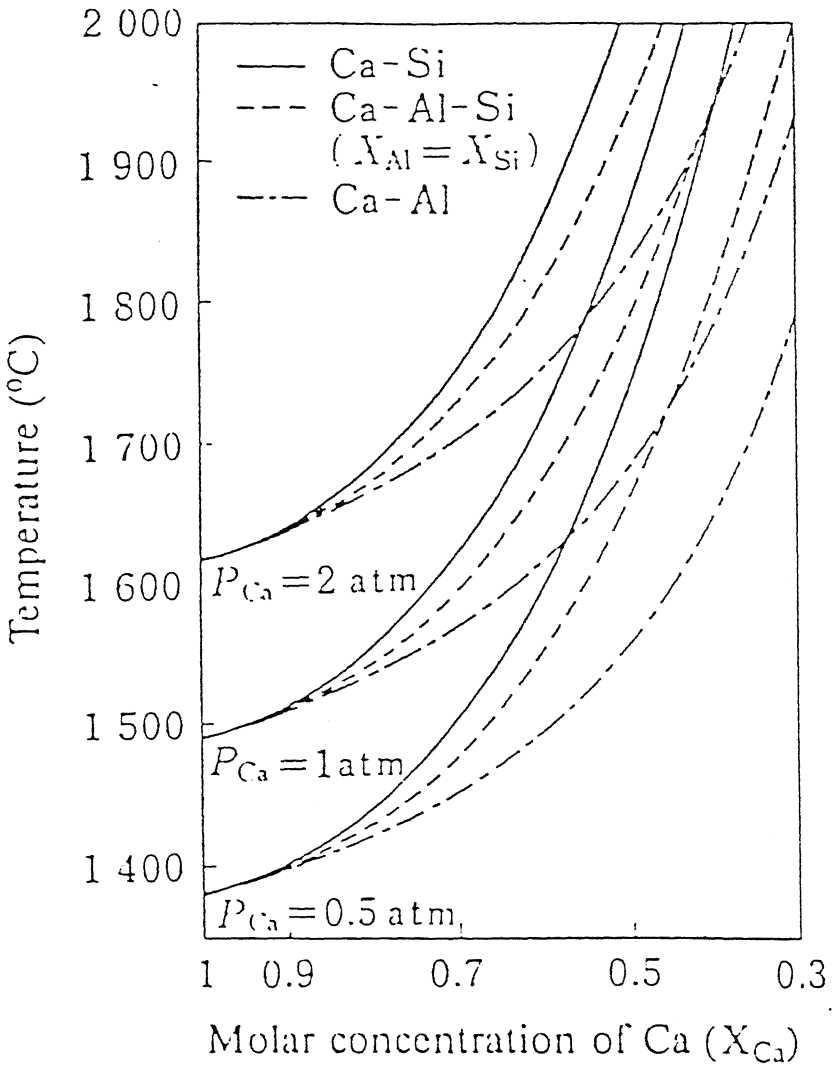

Figure 2.1: Influence of the molar concentration of Ca on the boiling point at various pressures.

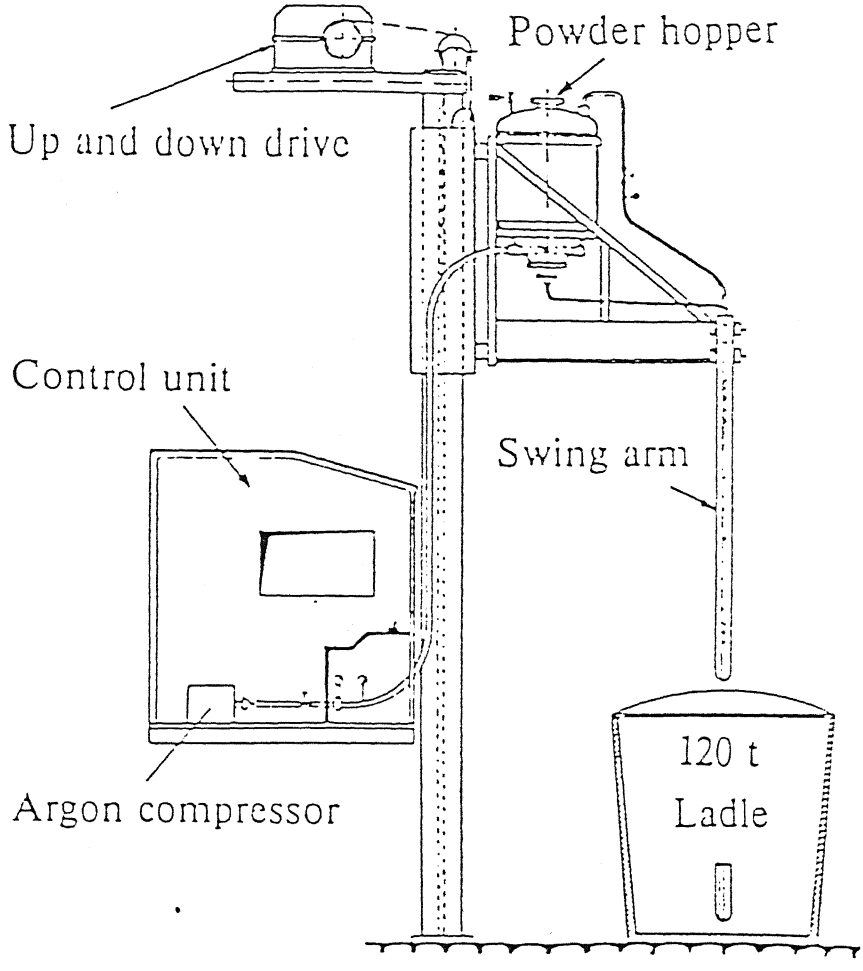

Figure 2.2: Schematic diagram of T.N. Lance.

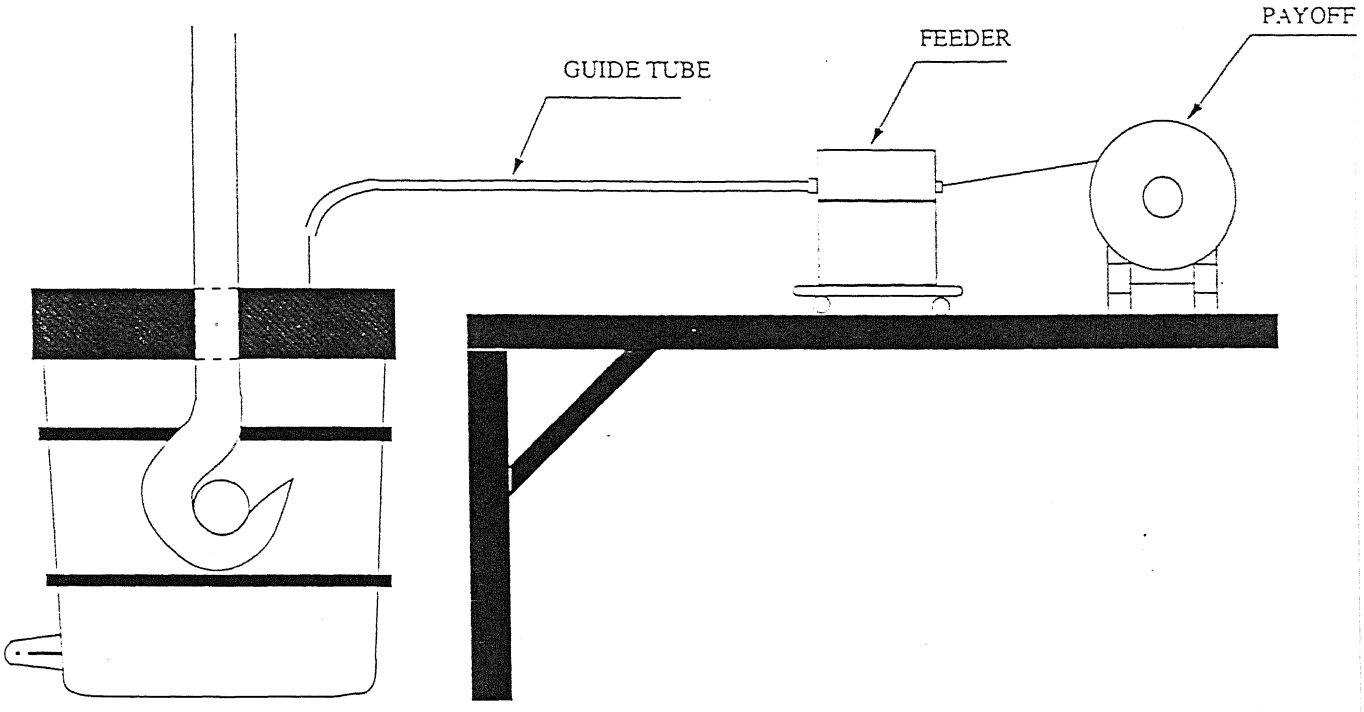

Figure 2.3: Schematic diagram of Wire Injection method.

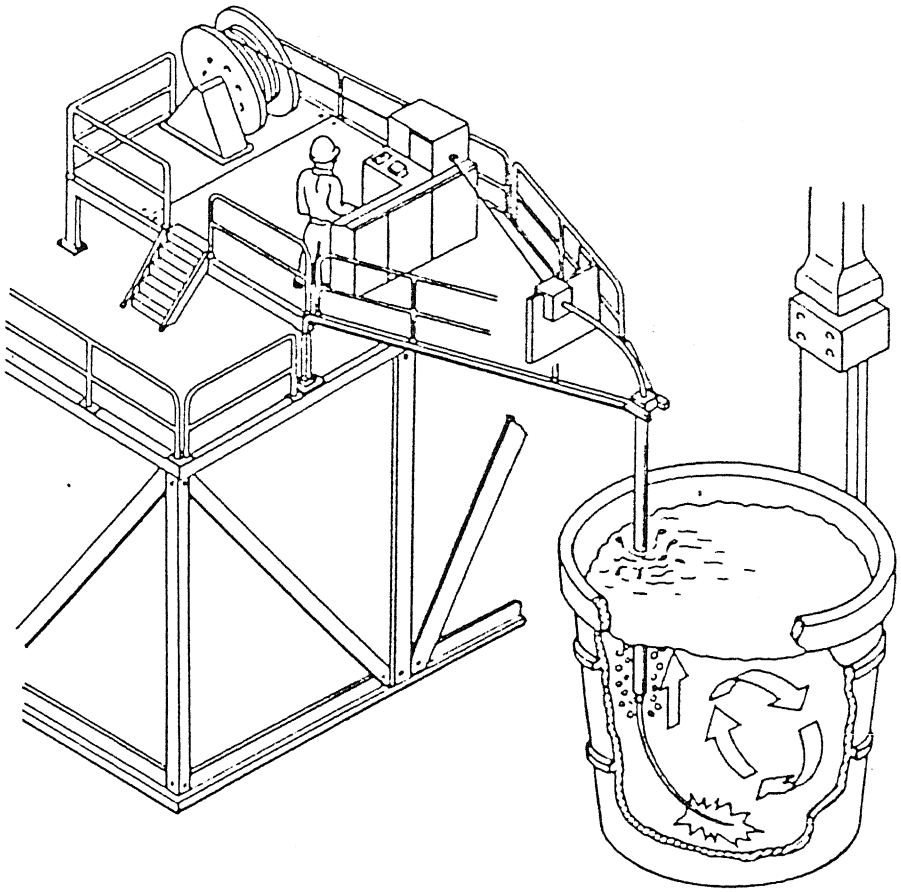

Figure 2.4: Schematic diagr

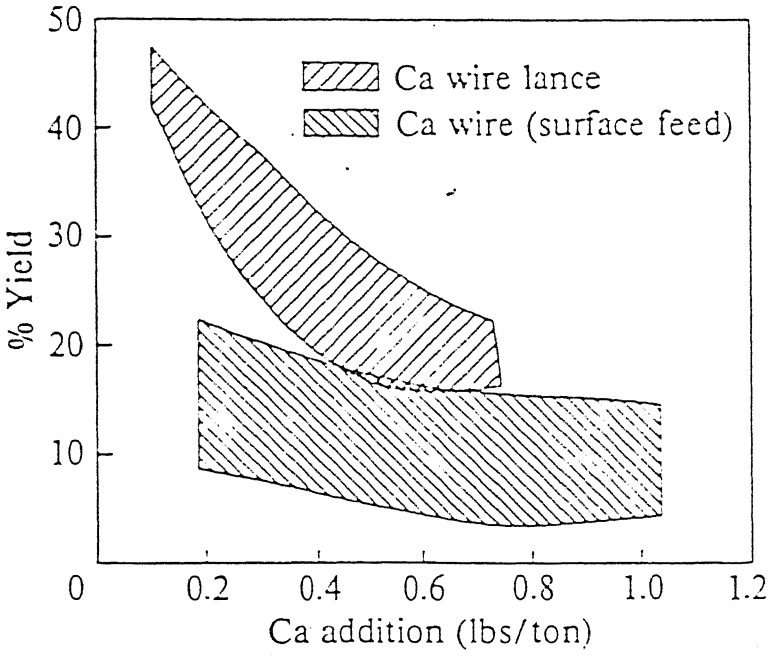

Figure 2.5: Comparison of calcium yield between Wire lance and Wire injection methods.

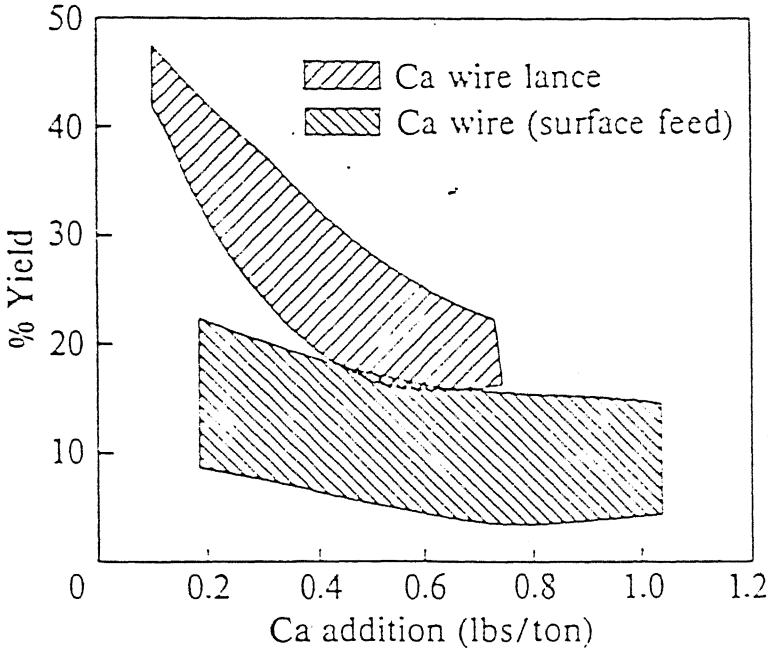

Figure 2.5: Comparison of calcium yield between Wire lance and Wire injection methods.

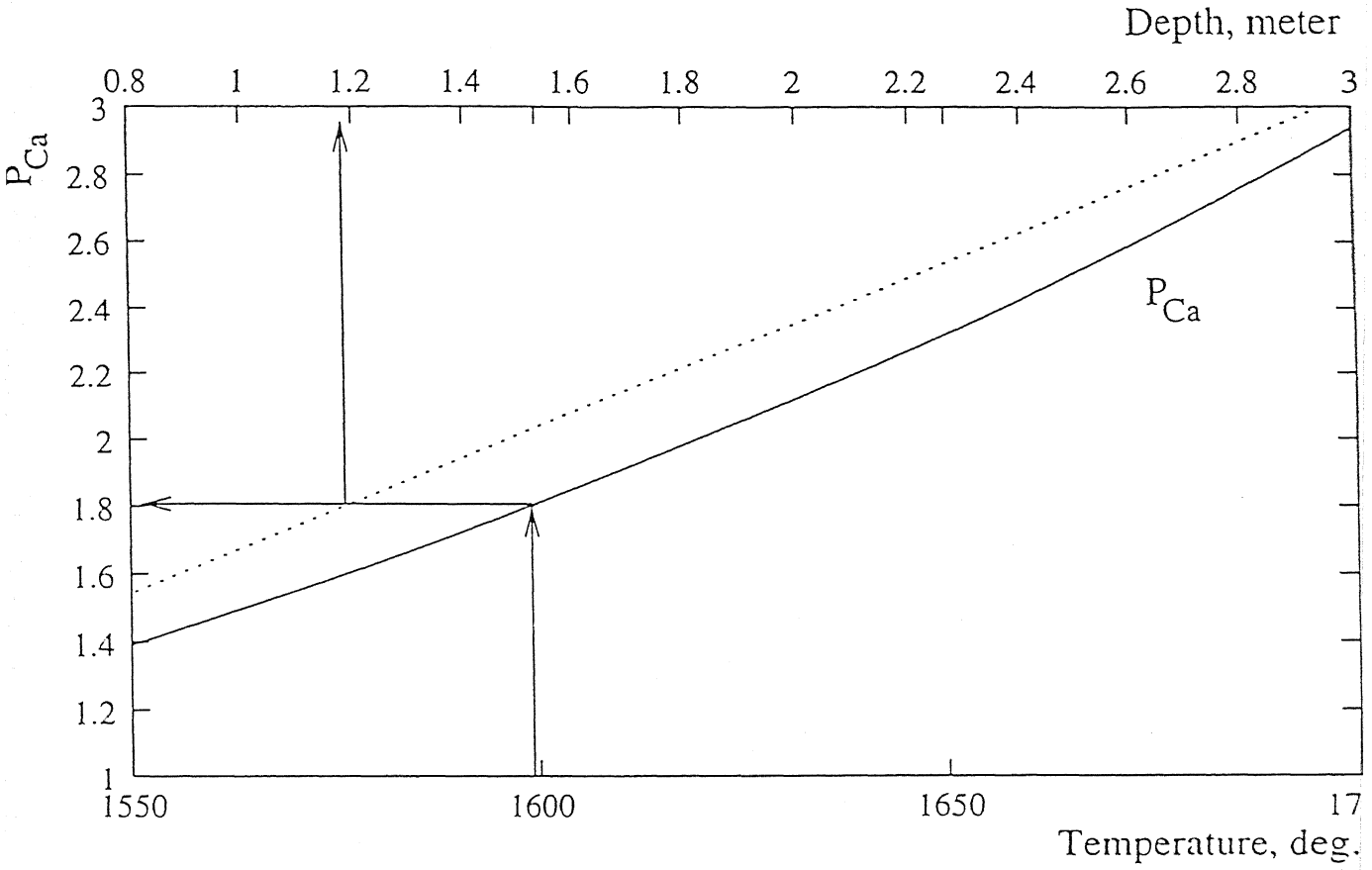

Figure 2.6: Vapour pressure of calcium as a function of temperature and the ferro-static head.

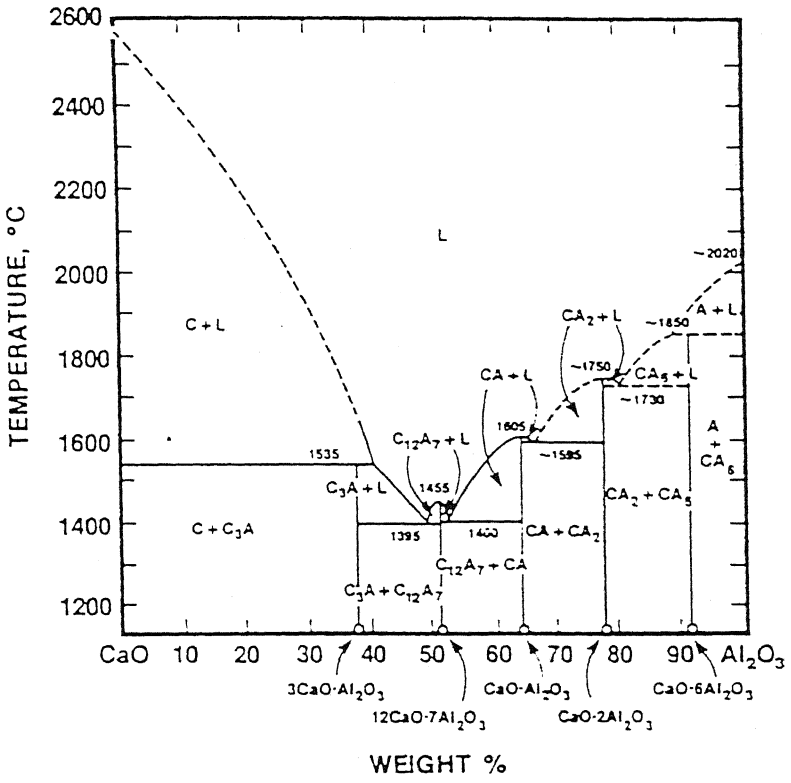

Figure 2.7: $CaO - Al_2O_3$ binary phase diagram.

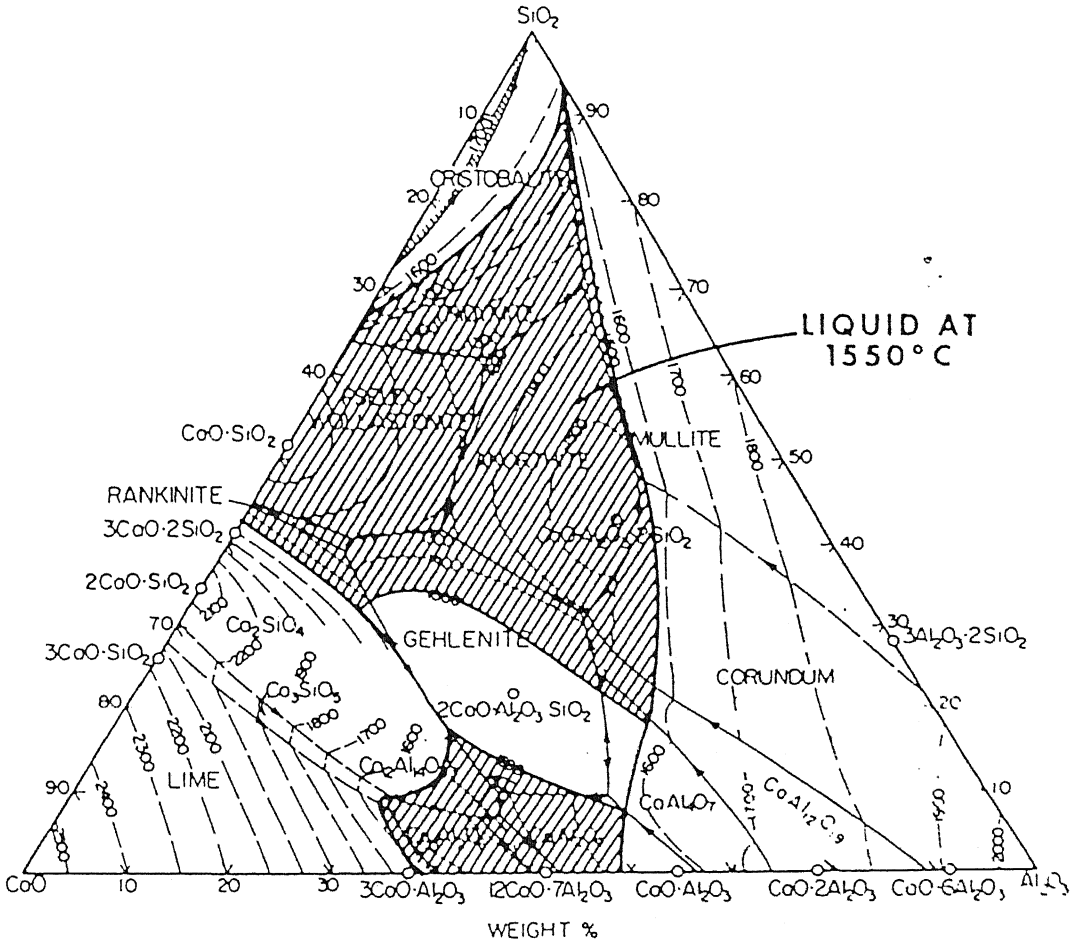

Figure 2.8: $CaO - Al_2O_3 - SiO_2$ ternary phase diagram at 1823K.

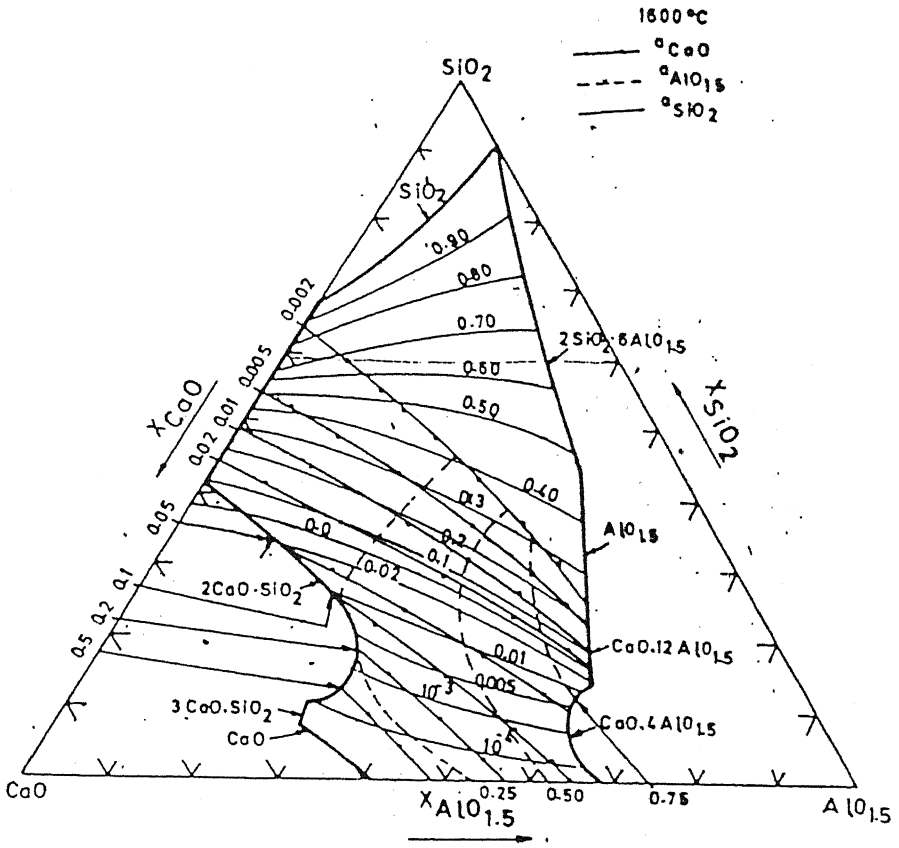

Figure 2.9: $CaO - Al_2O_3 - SiO_2$ iso-activity ternary diagram.

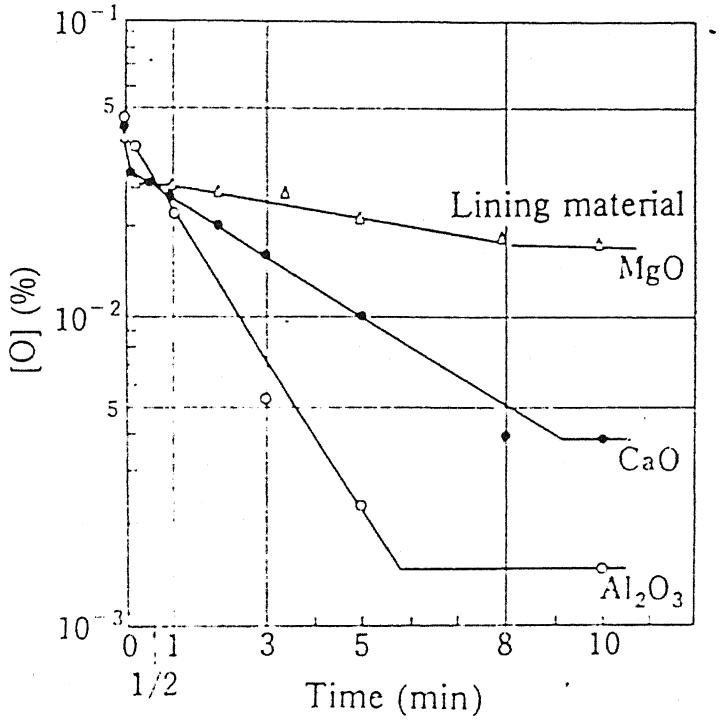

Figure 2.10: Influence of the lining materials on the change of [O] in iron after calcium addition.

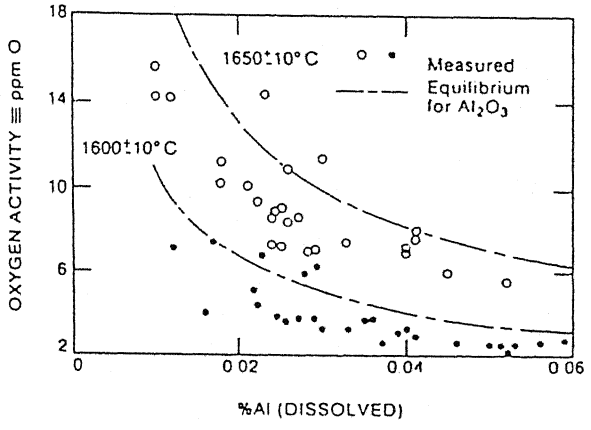

Figure 2.11: Dissolved O_2 after aluminum deoxidation and hard argon stirring.

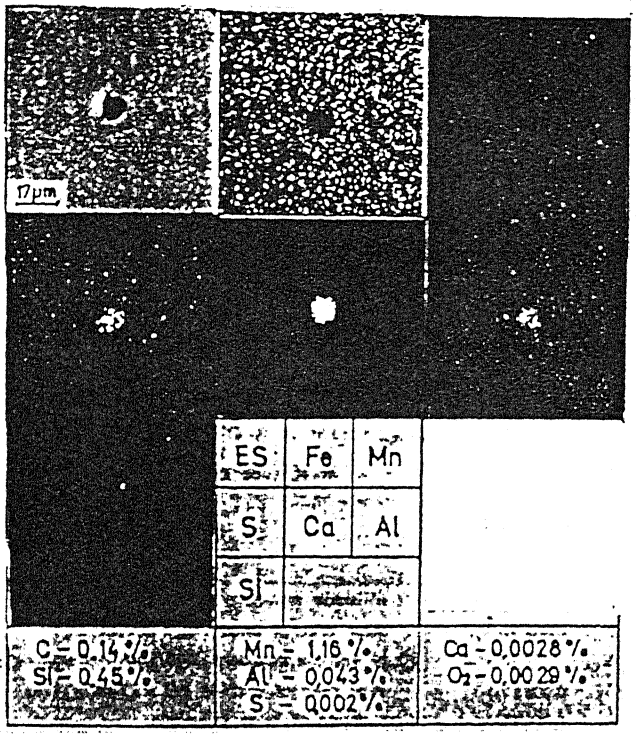

Figure 2.12: Single phase modified inclusion

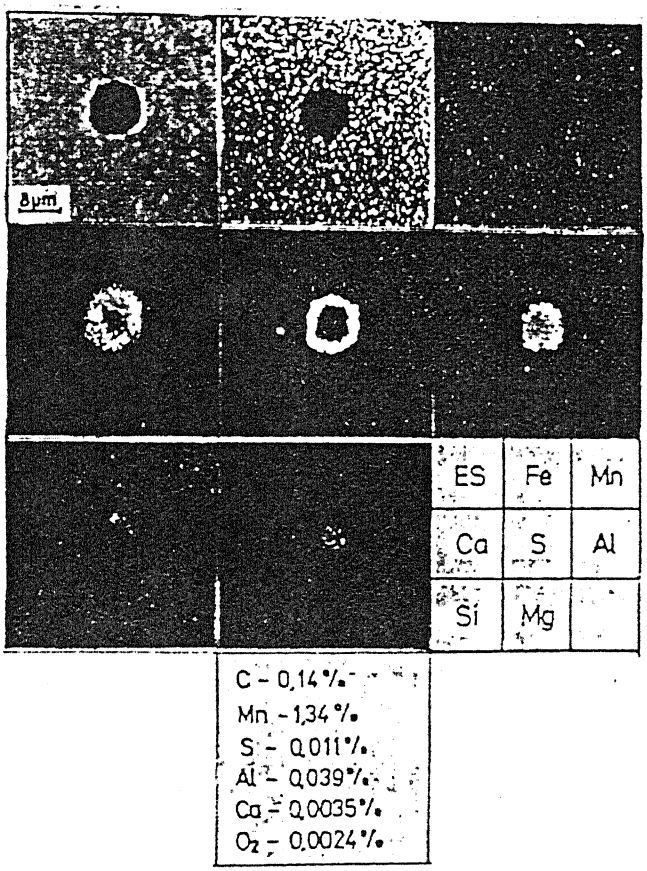

Figure 2.13: Duplex $CaO\text{-}Al_2O_3$ inclusions with thin CaS layer

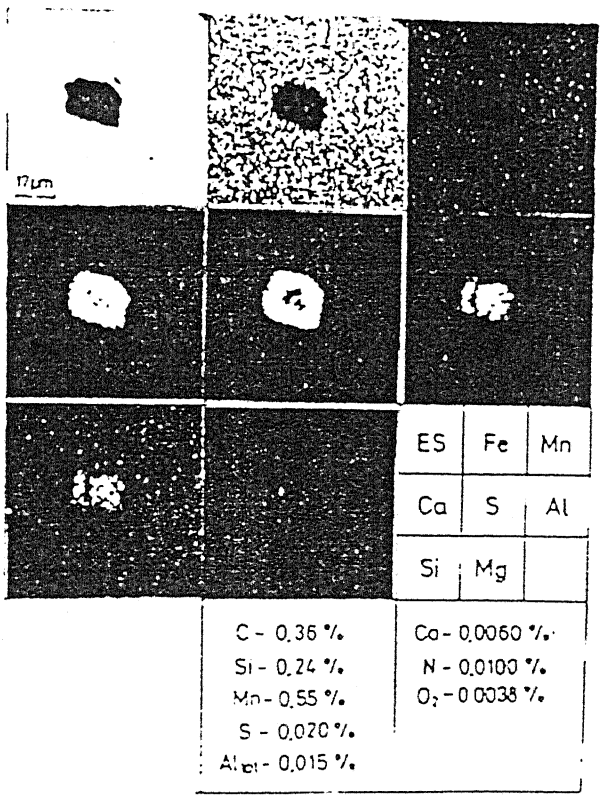

Figure 2.14: CaO- Al_2O_3 inclusions with thick CaS layer.

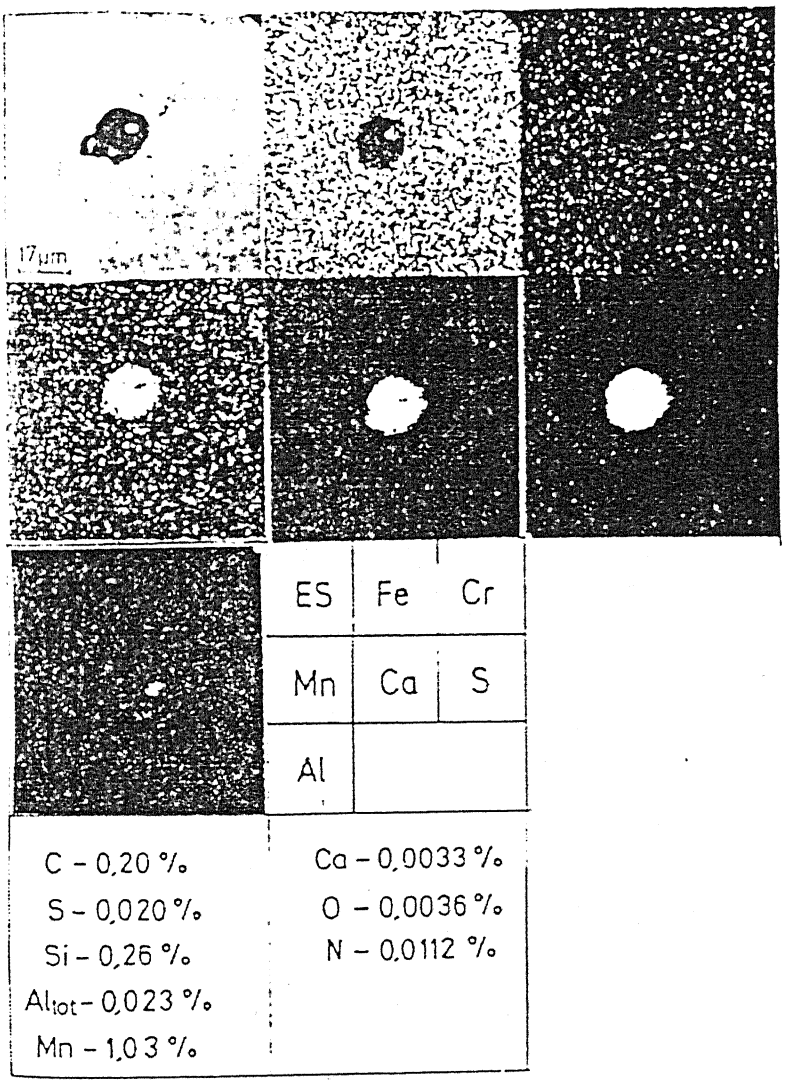

Figure 2.15: CaS-MnS inclusion

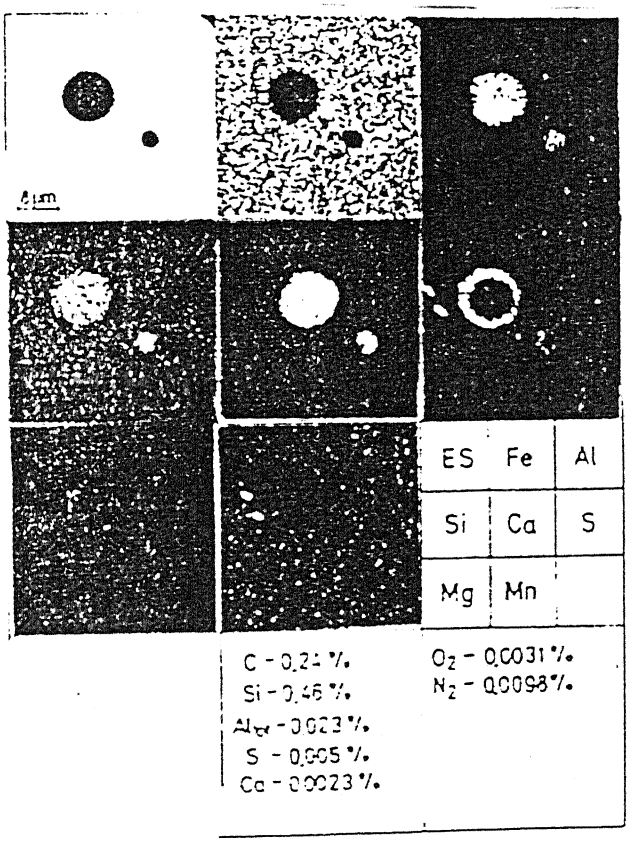

Figure 2.16: Complex calcium aluminate with Si and Mn.

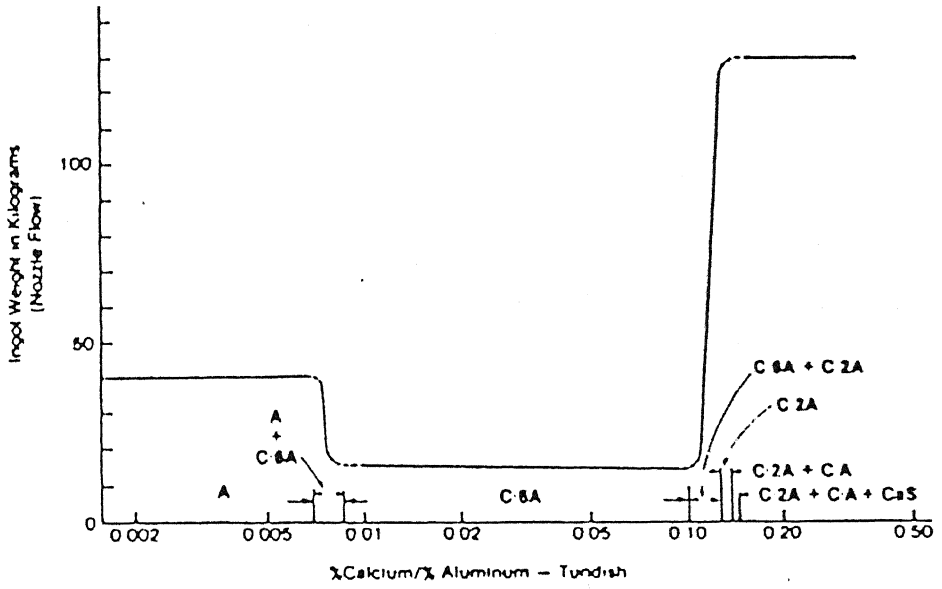

RELATIONSHIP OF NOZZLE FLOW TO TUNDISH CHEMISTRY AND INCLUSION PHASES. C REPRESENTS CaO AND A, Al_2O_3.

Figure 2.17: Relationship of nozzle flow to increase in inclusion volume.

CHAPTER 3

INJECTION PRACTICE AT TATA STEEL

3.1 Introduction

Powder based lance injection as well as wire injection is employed for calcium alloy injection in the steel ladle at LD Shop 1 of TATA STEEL. Approximately 90 % of the product mix are teemed via continuous casting route. Out of this approximately 60 % of the silicon-manganese killed grade is treated with CaSi (30/60)(see Table 1.2 for other details) while the rest are teemed without any injection treatment. EWNR constitutes approximately 10 % of the total continuously cast product mix and is treated with CaFe (30/70) wire.

As, already discussed in chapter 2, in order to ensure a good drawability the residual oxygen content of liquid steel prior to casting should be low so that billets are free from blow holes and / or pinholes. Following calcium based alloy is injected into liquid steel with a view to obtain low residual oxygen content:

- CaSi for low C - Si - Mn killed steels
- CaFe for Low C - Low Si - Low Al steels

In the plant practice at TATA STEEL, the liquid steel is tapped in a 130-ton basic lined (dolomite) ladle from bottom stirred LD converter. Bulk of the ferro - alloys are added in the ladle while tapping. A preliminary mixing and homogenization of liquid steel is done by top lance argon stirring at the "On Line Purging (OLP)" station for approximately three minutes. The gas flow rate employed at OLP is generally 150 liters per minute. Physical model studies as well as plant trials carried out at TATA STEEL [24] have shown that argon purging duration between 2 to 3 minutes (at a flow rate of 150 liters per minute with a three hole lance) is sufficient to obtain a satisfactory homogenization with respect to chemical composition. At the end of stirring a metal sample is taken, dissolved oxygen is measured using CELOX, and a separate temperature probe is used for accurate measurement of temperature. Hereafter, the ladle is shifted to "Argon Rinsing Station (ARS)" for calcium alloy injection and final composition

adjustment. Analysis of the sample collected at OLP is used to decide the trimming additions of ferro - alloys at ARS and temperature and oxygen readings obtained at OLP are used to decide the amount of calcium to be injected and the duration of stirring. The dissolved oxygen level at the end of treatment varies from 40 to 50 ppm (see Figure 3.1 for End-treatment dissolved oxygen frequency distribution). The LD converter at Shop1 TATA STEEL does not have slag stopper device. Absence of slag stopper device in the LD Converter is compensated by the following means:

- By maintaining a run - out time (i.e. tapping duration) between 4 - 6 minutes.
- Termination of tapping by leaving behind a portion of steel in the converter.

In spite of these steps, however, a small amount of converter slag is carried over into the ladle during tapping. Also, sometimes the ladles are not fully clean at the time of tapping i.e. free from accumulated slag. Absence of ladle furnace, occasional inappropriate addition of ladle covering reagent, delay in dumping ladle slag after casting are some of the reasons which results in the solidification of ladle slag at the end of casting hence its retention in the ladles.

3.2 Specimen Preparation Procedure and S.E.M. Examination Details

In the present work ladle samples were collected from eighteen heats (one sample from each cast) after approximately 3 - 5 minutes of calcium injection. Fifteen tundish samples (one sample from each cast) were also collected after approximately 30 minutes of start of continuous casting (total casting duration: 80 minutes). These samples were marked and cut to size and polished by successive wet grinding on 100, 150, 240, 320, 400, 500 and 600 grit silicon carbide papers and finally polishing on nylon cloth using diamond paste and using sufficient lapping oil to keep the cloth moist. At the end, samples were washed with water, dried and stored in desiccator.

Scanning Electron Microscopic (SEM) examination was conducted on these samples. Energy dispersive X-Ray spectrometer (KEVEX - JEOL 6400) was used for

spot analysis. Element mapping of inclusions was done to ascertain the inclusion type and composition.

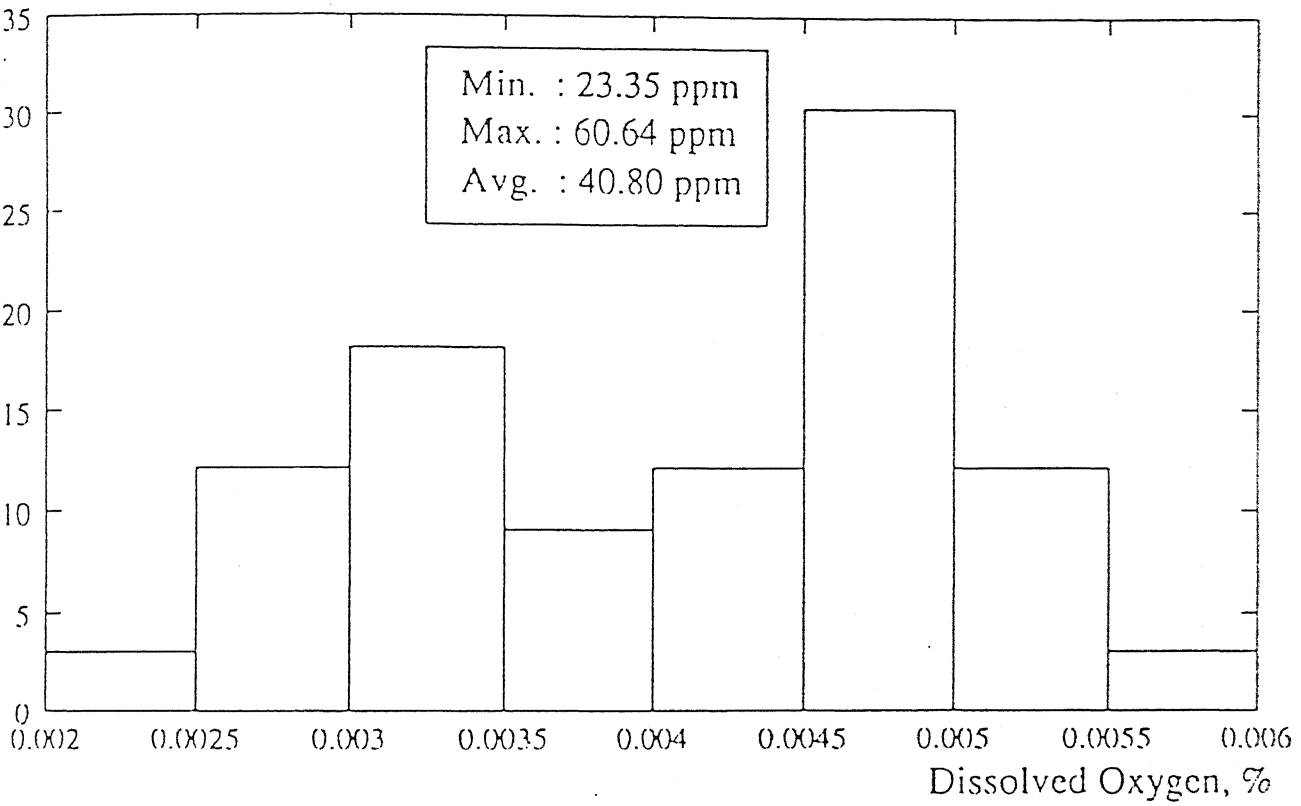

Figure 3.1: Frequency distribution of dissolved oxygen at the end of treatment.

CHAPTER 4

RESULTS AND DISCUSSIONS

4.1 Introduction

In this chapter, the result of chemical analysis of steel samples and scanning electron microscope investigations are first discussed to decide the limits of composition (dissolved Ca, Al, O in metal and CaO and Al_2O_3 contents of slag) and also the inclusions present in the steel. A thermodynamic model is then used to check the existence of thermodynamic equilibrium between metal, slag and inclusion by using the published values of interaction parameters and equilibrium constants. As mentioned in section 1.3, considerable differences exist (of several orders of magnitude) in the published thermodynamic data on Fe - Ca - Si - Al - O / CaO - FeO - SiO_2 - Al_2O_3 system. New values of interaction parameters and equilibrium constants are estimated on the basis of data collected in the present work by using a procedure suggested by Gustaffson and Mellberg [6]. Genetic Algorithmic Search (GAS) procedure is then used to countercheck the estimated thermodynamic parameters.

Frequency distribution of residual calcium in EWNR grade is shown in Figure 4.1. Figure 4.2 shows the adverse effect of LD converter's slag carry over (measured by an increase in phosphorous content, between tap analysis and ladle sample analysis (LSA) collected at the end of injection treatment, by $\geq$ 0.005 %) on the recovery of calcium in EWNR grade of steel. It can be seen from Figure 4.2 that slag carry over results in a significant lowering of total residual calcium in steel for a given calcium addition. Also, the total residual calcium shows a decreasing trend after attaining a maximum value (e.g. residual calcium level of 70 ppm achieved at 1.75 kg/ton of calcium addition). Pellicani [25] et al. reported that there is a possibility that when dissolved calcium increases it also reacts with refractories. Therefore, a competition between inclusions and refractories for the absorption of dissolved calcium takes place.

4.2 Scanning Electron Microscopic Observations of Samples

Steel samples collected from the ladle 3 to 5 minutes after the end of Ca - Fe wire injection and also the samples taken from tundish were examined on SEM. It was observed that:

(i) Area fraction of inclusions (obtained by Quantimeter Image Analyzer Q – 970) was high in most of the samples (see Table 4.1); it varied between 0.109 (minimum) to 0.25 (maximum) (**Average: 0.15988**) in the ladle samples and from 0.087 (minimum) to 0.130 (maximum) (**Average: 0.105**) in the tundish samples.

(ii) Approximately 95 % (by volume) of the inclusions observed in all the samples were FeO - SiO_2 type and their size range varied from 10 - 30 μ m (see Figure 4.3)

(iii) Remaining inclusions were complex oxides of elements such as Zr, Ca, Al, Si, Mn and Mg. Size fraction of such inclusions varied between 1 - 3 μ m (see Figure 4.4)

(iv) Complex Oxides were found to contain sulphur in the following three forms:

(a) As thin layer at the periphery of the inclusions. (Figure 4.5)

(b) As thick layer at the periphery of the inclusions. (Figure 4.6)

(c) Uniformly distributed within the inclusion matrix. (Figure 4.7)

The source of zirconium in the inclusions may be attributed to the presence of zirconium in the steel samplers, which is provided essentially to deoxidize the steel sample for an accurate chemical analysis on Optical Spectroscope. A non-porous sample thus obtained helps in correctly determining the nitrogen content (total) of steel sample. Since the volume fraction of CaO - Al_2O_3 - SiO_2 type inclusion in the samples was small, it may be concluded that both calcium and aluminum mass percentages as determined by optical spectroscopic analysis represent dissolved calcium and aluminum present in liquid steel. The reported silicon mass percentage in these samples will include the silicon present in FeO - SiO_2 inclusions as well. Thus, the soluble silicon content of steel is expected to be slightly lower than the reported mass percentage of silicon as determined by optical spectroscopic analysis.

A low inclusion area fraction in tundish samples as compared to ladle samples indicates that part of the inclusion floated up with time. Some inclusions are also expected to float in the ladle during the casting operation.

It has been suggested [26] that large sized inclusions (10 - 30 μ m) in the ladle samples are essentially a result of reoxidation of steel during tapping, purging operations and reaction of metal with LD carryover slag. These types of inclusions typically contain high concentrations of weak deoxidizers and are relatively bigger in size.

4.3 Assessment of Slag Metal Equilibrium on the Basis of Published Thermodynamic Data

Ladle slag consisted primarily of CaO, SiO_2 and Al_2O_3 and the metal phase contained Fe, C, S, Ca, Si, Al, O. As a first approximation it is assumed that slag and metal phases approach equilibrium within 3 - 4 minutes of Ca - Fe wire injection. This is based on the plant observation that dissolved oxygen measured by CELOX after 3 – 4 minutes of Ca-Fe injection does not significantly change with time.

For a known slag analysis (i.e. mass percentages of CaO - SiO_2 - Al_2O_3) - the activities of CaO, SiO_2 and Al_2O_3 can be directly read off from iso-activity ternary diagram of either Rein and Chipman[10] or, Ohto and Suito[27]. Equilibrium composition (with respect to dissolved calcium, silicon and aluminum in steel) can be calculated by using a thermodynamic model.

Thermodynamic model [37]:

The steps of the calculations are:

(i) Equilibrium constant and first order interaction parameters are selected from Table 4.2.

(ii) From measured oxygen activity [h_O] the values of [h_{Ca}], [h_{Si}] and [h_{Al}] are calculated using the following relations:

$$[Ca] + [O] = CaO\ (s)$$

$$2[Al] + 3[O] = Al_2O_3(s)$$

$$[Si] + 2[O] = SiO_2\ (s)$$

$$h_{Ca} = {}^{a}CaO\ /\ (K_{Ca} \times h_O)$$

$$h_{Al} = {}^{a}Al_2O_3\ /\ (K_{Al} \times (h_O{}^3))$$

$$h_{Si} = {}^{a}SiO_2\ /\ (K_{Si} \times (h_O{}^2))$$

(iii) Equilibrium metal composition (in mass percentage) is calculated by simultaneous solution of following four equations in four unknowns (mass % Ca, mass % Al, mass % O and mass % Si) by using an iterative procedure.

$$\log_{10}(\text{mass \% Al})_{equilibrium} = [\log_{10}h_{Al} - (e_{Al}{}^{Al} \times \text{mass \% Al}) - (e_{Al}{}^{Ca} \times \text{mass \% Ca}) - (e_{Al}{}^{O} \times \text{mass \% O}) - (e_{Al}{}^{Si} \times \text{mass \% Si})] \quad (4.1)$$

$$\log_{10}(\text{mass \% Si})_{equilibrium} = [\log_{10}h_{Si} - (e_{Si}{}^{Al} \times \text{mass \% Al}) - (e_{Si}{}^{Ca} \times \text{mass \% Ca}) - (e_{Si}{}^{O} \times \text{mass \% O}) - (e_{Si}{}^{Si} \times \text{mass \% Si})] \quad (4.2)$$

$$\log_{10}(\text{mass \% Ca})_{equilibrium} = [\log_{10}h_{Ca} - (e_{Ca}{}^{Al} \times \text{mass \% Al}) - (e_{Ca}{}^{Ca} \times \text{mass \% Ca}) - (e_{Ca}{}^{O} \times \text{mass \% O}) - (e_{Ca}{}^{Si} \times \text{mass \% Si})] \quad (4.3)$$

$$\log_{10}(\text{mass \% O})_{equilibrium} = [\log_{10}h_O - (e_O{}^{Al} \times \text{mass \% Al}) - (e_O{}^{Ca} \times \text{mass \% Ca}) - (e_O{}^{O} \times \text{mass \% O}) - (e_O{}^{Si} \times \text{mass \% Si})] \quad (4.4)$$

In the numerical algorithm developed in this work, the initial guesses for mass % Al, mass % Si, mass % Ca and mass % O to be used in the R.H.S. are obtained by using an iterative procedure. To start with Eq.(4.1) is solved. An initial guess for mass % Al is made (say 0.0001). Other mass percentages are assumed to be zero (i.e. mass % Si, mass % Ca & mass % O). The calculated value of mass % Al and h_{Al} (calculated in the previous step) is substituted in R.H.S. of Eq.(4.1) and is called F (Al). Now, Eq. (4.1) is differentiated with respect to mass % Al and is termed as F' (Al). The value of F' (Al) is obtained by inserting first estimate of mass % Al. F (Al)/F' (Al) is subtracted from first estimate to evaluate a new value of mass % Al. Now, this new value of mass % Al is

compared with the old value of mass % Al and error value is compared with present error limit (i.e. Convergence criteria). If convergence criteria are not met with then the old value of mass % Al is replaced with the new value of mass % Al. This procedure is repeated till error becomes equal to or, less than the convergence criteria. In the next step Eq. (4.2) is considered where the converged value of mass % Al obtained in the previous step is substituted and an estimate of initial guess for mass % Si is made (say 0.0001 %). Again, a value of zero is assigned to the remaining mass percentages (i.e. mass % Ca, mass % O).

Again, a similar iterative procedure (as followed for obtaining mass % Al) is followed for obtaining estimates of mass % Si, mass % Ca and mass % O.

Having obtained all the first estimates of mass % Al, mass % Si, mass % Ca and mass % O the calculation is restarted from Eq. (4.1) but this time with the calculated mass %s of respective elements.

This procedure is repeated until the values converge according to the error limit set in the program.

A FORTRAN-77 computer code incorporating the above procedure is given in Annexure # 1.

4.3.1 Results of thermodynamic model using published values of interaction parameters and equilibrium constants.

Ladle slag samples collected 3 – 4 minutes after the Ca-Fe injection treatment showed that the major constituents were CaO, SiO_2 and Al_2O_3 and their normalized values have been plotted on a ternary diagram (Figure 4.8). The corresponding activities of CaO, SiO_2 and Al_2O_3 were read from two sources separately: (i) Rein & Chipman's[10] (Figure 4.9a) and, (ii) Ohto & Suito's[27] (Figure 4.9b) CaO - SiO_2 - Al_2O_3 iso activity diagram at 1873 K (see Table 4.3). Error in reading the activity values from the ternary diagram is of the order 5×10^{-3} for CaO and Al_2O_3 and 5×10^{-4} for SiO_2. It is evident from Figure 4.8 that few slag samples lie in the two - phase region (solid - liquid) of the ternary diagram (see point **A**). The following procedure is adopted to estimate activities: A tie line joining the CaO corner and the point **A** representing the slag constituent on the

ternary diagram is extended till it reaches the liquid phase boundary (point B). Activities of CaO, SiO_2 and Al_2O_3 corresponding to B are read directly from the figure.

Interaction parameters and equilibrium constants as reported by Gaye and Gatellier and those of Sigworth and Elliott are compiled in Table 4.2.A comparative example, between actual metal analysis and the calculated analysis, is shown in following tables. Comparisons between actual metal analysis and that calculated from thermodynamic model (see Table 4.4) show considerable disagreement.

H.No.	Calcium, mass %				
	Actual analysis	Calculated Analysis			
		Elliot and Sigworth		Gaye and Gatellier	
		Rein & Chip.	Ohto & Suito	Rein & Chip.	Ohto & Suito
29501	0.0036	0.0317	0.0145	0.3433	0.1372
35238	0.0024	0.0041	0.0060	0.0109	0.0160

H.No.	Silicon, mass %				
	Actual analysis	Calculated Analysis			
		Elliot and Sigworth		Gaye and Gatellier	
		Rein & Chip.	Ohto & Suito	Rein & Chip.	Ohto & Suito
29501	0.018	0.0007	0.0007	0.0007	0.0007
35238	0.020	0.0144	0.1925	0.0144	0.1938

H.No.	Aluminum, mass %				
	Actual analysis	Calculated Analysis			
		Elliot and Sigworth		Gaye and Gatellier	
		Rein & Chip.	Ohto & Suito	Rein & Chip.	Ohto & Suito
29501	0.005	0.0003	0.0003	0.0009	0.0009
35238	0.005	0.0005	0.0004	0.0017	0.0013

This confirms a need for re-estimation of equilibrium constants and interaction parameters on the basis of data obtained in present work for EWNR steels.

4.4 Thermodynamic Model for the Simultaneous Determination of Interaction Parameters and Equilibrium Constants. [6]

A deoxidation or, desulphurisation reaction can be represented in general form as:

$$i_a j_b \rightarrow a \times i + b \times j$$

for the above reaction we have,

$$\log_{10} K = (a \times \log_{10} h_i) + (b \times \log_{10} h_j)$$

where Henerian standard state of 1 mass % is assumed for the dissolved elements. If only first order interaction parameters are considered and self interaction is ignored (as a first approximation) then activity coefficients f_i and f_j can be written as:

$$\log_{10} f_i = e_i^j \times (\text{mass \% j})$$

$$\log_{10} f_j = e_j^i \times (\text{mass \% i})$$

thus,

$$\log_{10} K = \log_{10}[(\%i)^a \times (\%j)^b] + a \times e_i^j + b \times e_j^i$$

Introducing k' (the apparent solubility product)

$$k' = [(\%i)^a \times (\%j)^b]$$

and, also using the relation (Given by Lupis [28])

$$e_j^i = M_j / M_i \times e_i^j + (0.434 \times 10^{-2})[M_i + M_j / M_i]$$

or,

$$e_i^j = M_j / M_i \times e_j^i$$

we obtain, after rearranging :

$$- \log_{10} k' = - \log_{10} K + (e_i^j \times (\% j) \times a) + ((M_j / M_i) \times (\% i) \times b)$$

or,

$$- \log_{10} k' = - \log_{10} K + e_i^j \times z$$

where,

$$z = a \times (\%j) + b \times (M_j / M_i) \times (\%i)$$

Thus, if $- \log_{10} k'$ is plotted against composition, as shown in Figure 4.10[6], and the experimental data fall on a straight line then slope would be equal to e_i^j and intercept will give $- \log_{10} K$. However, if experimental data do not show this linear behavior, it would indicate that a first order interaction parameter alone does not describe the system adequately along the solubility line. The evaluation of interaction parameters with the help of the plot shown in Figure 4.10, has the following advantages:

a) Any inconsistency between the values assigned to the interaction parameter and the equilibrium constant would be easily revealed.

b) The range of applicability of first order interaction parameter only can be obtained directly.

c) The linear relation is valid even in the case of a substantial interaction both from i on j and j on i and simplifies the evaluation of experimental data.

d) The structure of the composition coordinate may be used to estimate the significance of either of the two mutual interaction effects. For instance, if

$$\{a \times (\%j)\} \gg \{b \times (M_j / M_i) \times (\%i)\}$$

with in the composition range of interest, then interaction from i on j may be neglected and vice versa.

4.4.1 Simultaneous Estimation of e_O^{Al} and $^{K}_{Al_2O_3}$ on the basis of Aluminum-Oxygen equilibrium before wire injection

As discussed in section 3.1, Aluminum bars are added (approximately 200 kg/ 130 ton of steel) in the ladle for primary deoxidation at the time of tapping of liquid steel. Depending on the dissolved oxygen and extent of reoxidation during tapping steel, pure

alumina inclusions may form. In the following calculation procedure (based on the Thermodynamic Model concepts explained in section 4.4) it is assumed for the sake of simplicity that alumina inclusion formed at this stage is in equilibrium with metal composition (determined by O.L.P. analysis - shown in Table 4.5). Dissolved oxygen content is measured with the help of CELOX probe after three minutes of Argon purging at O.L.P. Average temperature at O.L.P. is found to be 1665°C. Therefore, average temperature for the present calculation was assumed to be 1665°C for all the heats.

Aluminum deoxidation of liquid steel is represented by:

$$Al_2O_3\ (s) = 2\ [Al] + 3\ [O]$$

$$^{K}_{Al_2O_3} = (h_{Al}^{\ 2} \times h_O^{\ 3}) / {}^{a}_{Al_2O_3}$$

Here,

$$^{a}_{Al_2O_3} = 1.0 \quad \text{for pure Alumina.}$$

$$\log_{10} {}^{K}_{Al_2O_3} = 2.0 \times \log_{10}(h_{Al}) + 3.0 \times \log_{10}(h_O)$$

$$= [2 \times \log_{10}(f_{Al})] + [2 \times \log_{10}(\text{mass \% Al})] + [3 \times \log_{10}(f_O)] + [3 \times \log_{10}(\text{mass \% O})]$$

or,

$$\log_{10}({}^{K}_{Al_2O_3}) + [2.0 \times \sum (e_{Al}^{\ i} \times \text{mass \% i})] + [(3.0 \times \sum (e_O^{\ j} \times \text{mass \% j})]$$
$$= -e_{Al}^{\ O}[(2 \times \text{mass \% O}) + (1.78 \times \text{mass \% Al})] - \log_{10}[(\text{mass \% O})^{3.0} \times (\text{mass \% Al})^{2.0}]$$

Now, let

$$X = [(2 \times \text{mass \% O}) + (1.78 \times \text{mass \% Al})] \qquad (4.5)$$

$$Y = \log_{10}[(\text{mass \% O})^{3.0} \times (\text{mass \% Al})^{2.0}] + [2.0 \times \sum (e_{Al}^{\ i} \times \text{mass \% i})] + [(3.0 \times \sum (e_O^{\ j} \times \text{mass \% j})] \qquad (4.6)$$

Here, i and j represent elements other than O and Al, respectively.

Values of interaction parameters used in the present calculation are given below [42]:

e_{Al}^{Al}	0.045
e_{Al}^{C}	0.091
e_{Al}^{S}	0.03
e_{Al}^{Si}	0.0056
e_{O}^{C}	-0.45
e_{O}^{S}	-0.0642
e_{O}^{Si}	-0.13
e_{O}^{O}	-0.176

Results of linear regression performed between X and Y values obtained in equations (4.5) and (4.6) are:

Correlation Co-efficient		0.974
Regression Coefficient	$-e_{Al}^{O}$	50. 34
Standard Error of Coefficient		2.14
Regression Constant	$-\log_{10} K_{Al_2O_3}$	-12.06
Standard Error of Constant		0.09

Comparison of deoxidation equilibrium constant thus obtained shows a good agreement with other reported values in literature by other researchers as shown below:

Equilibrium Constant	At 1665°C
62780 / temp - 20.54 [45]	11.85
47400 / temp - 12.32 [51]	12.14
64000 / temp - 20.57 [49]	12.45
49696/ temp – 13.58[1]	12.06

4.4.2 Thermodynamic Model for Simultaneous Estimation of e_O^{Ca}, e_S^{Ca} and K_{CaO}

Plant data on metal analysis, slag analysis (see Table 4.3) and dissolved oxygen of EWNR steels is compiled in Table 4.6.

In the presence of solid CaO and solid CaS, the equilibrium constants for the reactions are given by Eqs. (4.7) and (4.8)

$$CaO(s) = [Ca] + [O]$$

$$K_{CaO} = (h_{Ca} \times h_O) / a_{CaO}$$

$$\log_{10}(K_{CaO}) = \log_{10}(k'_{CaO}) + \log_{10}(f_{Ca}) + \log_{10}(f_O) - \log_{10}(a_{CaO}) \quad (4.7)$$

$$CaS(s) = [Ca] + [S]$$

$$K_{CaS} = (h_{Ca} \times h_S) / a_{CaS}$$

$$\log_{10}(K_{CaS}) = \log_{10}(k'_{CaS}) + \log_{10}(f_{Ca}) + \log_{10}(f_S) - \log_{10}(a_{CaS}) \quad (4.8)$$

CaS being pure solid a_{CaS} is set equal to 1.

In dilute iron solution;

$$\log_{10}(f_{Ca}) = (e_{Ca}^{Ca} \times \text{mass \% Ca}) + (e_{Ca}^{S} \times \text{mass \% S}) + (e_{Ca}^{O} \times \text{mass \% O}) \quad (4.9)$$

$$\log_{10}(f_O) = (e_O^{Ca} \times \text{mass \% Ca}) + (e_O^{S} \times \text{mass \% S}) + (e_O^{O} \times \text{mass \% O}) \quad (4.10)$$

$$\log_{10}(f_S) = (e_S^{Ca} \times \text{mass \% Ca}) + (e_S^{S} \times \text{mass \% S}) + (e_S^{O} \times \text{mass \% O}) \quad (4.11)$$

Using interaction parameters, e_O^O, e_S^O, e_S^S (-0.2, -0.27, -0.028 respectively) and Eqs. (4.7), (4.8), (4.9), (4.10), (4.11) we get the following equation:

$$-\log_{10}(k'_{CaO}) - [1.25 \times e_S^{Ca} \times \text{mass\%S}] + [0.2065 \times \text{mass\%O}] + [0.136 \times \text{mass\%S}] + \log_{10}(a_{CaO})$$
$$= -\log_{10}(K_{CaO}) + e_O^{Ca}[(\text{mass \% Ca}) + (2.5051 \times \text{mass \% O})]$$

Let,

$$X = \{(\text{mass \% Ca}) + (2.5051 \times \text{mass \% O})\}$$

$$Y = -\log_{10}(k'_{CaO}) - [1.25 \times e_S^{Ca} \times \text{mass\%S}] + [0.2065 \times \text{mass\%O}] + [0.136 \times \text{mass\%S}] + \log_{10}(a_{CaO})$$

---

[1] Present Work

Now, with an arbitrarily chosen value of e_S^{Ca} a linear regression analysis is performed between X and Y. The slope of line thus obtained represents the e_O^{Ca} and the intercept represents $-\log_{10}(K_{CaO})$. The above procedure is repeated with different chosen values of e_S^{Ca} (Tables 4.7a and 4.7b). Regression output corresponding to best correlation coefficient is accepted to be the final result. Table 4.8 summarizes the best results obtained by using slag activities by Rein & Chipman and Ohto & Suito.

It may be inferred from the linear regression analysis that the use of slag activities given by Ohto & Suito gives a higher correlation coefficient for the data used in the present work.

4.4.3 Thermodynamic model for determination of e_O^{Al} and $^{K}Al_2O_3$ after wire injection.

Aluminium deoxidation reaction in the presence of calcium can be represented as below:

$$3(CaO) = 3[Ca] + 3[O] \quad (a)$$

$$2[Al] + 3[O] = (Al_2O_3) \quad (b)$$

$$3(CaO) + 2[Al] = (Al_2O_3) + 3[Ca] \quad (c)$$

or,

$$\log_{10}K_{(c)} = 3 \times \log_{10}f_{Ca} + 3 \times \log_{10}(\text{mass\%Ca}) + \log_{10}{}^{a}Al_2O_3 - 3\times \log_{10}{}^{a}CaO - 2 \times \log_{10}f_{Al} - 2 \times \log_{10}(\text{mass\%Al})$$

where,

$$\log_{10}(f_{Ca}) = e_{Ca}^{Ca} \times (\text{mass \% Ca}) + e_{Ca}^{S} \times (\text{mass \% S}) + e_{Ca}^{O} \times (\text{mass \% O}) + e_{Ca}^{Si} \times (\text{mass \% Si}) + e_{Ca}^{C} \times (\text{mass \% C})$$

$$\log_{10}(f_{Al}) = e_{Al}^{S} \times (\text{mass \% S}) + e_{Al}^{Al} \times (\text{mass \% Al}) + e_{Al}^{C} \times (\text{mass \% C})$$

Now, let

$$Y = 3 \times \log_{10} f_{Ca} + 3 \times \log_{10}(\text{mass\%Ca}) + \log_{10} {}^{a}Al_2O_3 - 3 \times \log_{10} {}^{a}CaO - 2 \times \log_{10} f_{Al} - 2 \times \log_{10}(\text{mass\%Al})$$

$$X = 2 \times e_{Al}^{O} \times (\text{mass \% O})$$

Results of linear regression performed between X and Y values obtained above are (values of e_{Ca}^{S} and e_{Ca}^{O} used are compiled in TABLE 4.8, other interaction parameters used in the calculation are compiled in TABLE 4.2):

	$e_{Ca}^{O} = -308.38$ $e_{Ca}^{S} = -36.25$		$e_{Ca}^{O} = -25.0$ $e_{Ca}^{S} = -223.81$	
	Slag Activity : Rein & Chipman		Slag Activity : Ohto & Suito	
	Other Parameters[2]		Other Parameters[3]	
Correlation Coefficient	0.32	0.32	0.61	0.48
Reg. Coeff. (e_{Al}^{O})	-205.91	-205.91	-330.06	-223.96
Std. Error of Reg. Coeff.	107.81	107.80	77.08	72.73
Reg. Const. ($\log_{10}K_{(c)}$)	-5.086	-5.092	-3.811	-3.048
Std. Error of Reg. Const.	0.90	0.90	0.64	0.61

It can be seen that the best result has been obtained by using slag activities from iso-activity diagram by Ohto and Suito and interaction parameters by Gaye and Gatellier.

Now, Equilibrium constants for equations (a), (b), (c) are interrelated as shown below:

[2] Sigworth & Elliott [42]
[3] Gay & Gatellier [50]

$$K_a^3 \times K_b = K_c$$

Thus,

$$^{K}Al_2O_3 = K_b = 6.44 \times 10^{12}$$

Comparison of equilibrium constant ($^{K}Al_2O_3$) thus obtained shows a good agreement with values reported by other researchers as shown below:

Equilibrium Constant	At 1610°C
62780 / temp - 20.54 [45]	12.80
47400 / temp - 12.32 [51]	12.85
64000 / temp - 20.57 [49]	13.41
49696 / temp - 13.58[4]	12.81

Spot analyses of typical complex inclusion in three heats are shown in Figures 4.11, 4.12, and 4.13. Both inclusion spot analysis and slag analysis in these heats indicated that CaO, SiO_2 and Al_2O_3 were the major constituents (Table 4.9). Also, activities of CaO, SiO_2 and Al_2O_3, in the inclusion as well as slag, were found to be almost similar. This indicates that interaction parameters and equilibrium constants determined above (i.e. by considering metal – slag equilibrium) will hold good for metal – inclusion system and simultaneous equilibrium exist between metal, slag and inclusion.

4.5 Application of Genetic Adaptive Search Technique to Evaluate Interaction Parameters and Equilibrium Constants

INTRODUCTION

Genetic Adaptive search (GAS) or more commonly Genetic Algorithm (G.A.) is now a well-established optimization technique and ample literature is available on the subject [29,30]. In the present work G.A.is used to estimate the interaction parameter and equilibrium constants from experimental data by using the following procedure:

[4] Present work

Calcium based deoxidation and desulphurisation reactions are represented by Eqs. (4.7) and (4.8) (see Section 4.4.2). Now, for desulphurisation reaction – thirty-three different functions can be written, one for each set of observation i.e. for a particular cast number, by using metal compositions given in Table 4.6. The general format for these functions is given below:

$$F(i) = -\log_{10}(k'_{CaS}(i)) - \{2.5051 \times X_3 \times (\text{mass \% O(i)})\} - [X_1 \times \{\text{mass\%Ca(i)} + (1.25 \times \text{mass \% S(i)})\}] + X_4 + \{0.28144 \times \text{mass \% O(i)}\} + \{0.029085 \times \text{mass \% S(i)}\}$$

Similarly, for deoxidation reaction a second set of 33 functions may be written as given below:

$$F(j) = -\log_{10}(k'_{CaO}(i)) - \{1.25 \times X_1 \times (\text{mass \% S(i)})\} - [X_3 \times \{\text{mass\%Ca(i)} + (2.5051 \times \text{mass \% O(i)})\}] + X_2 + \{0.2065 \times \text{mass \% O(i)}\} + \{0.136085 \times \text{mass \% S(i)}\} + \log_{10}(a_{CaO})$$

where,

$$k'_{CaO} = (\text{mass \% Ca}) \times (\text{mass \% O})$$

$$k'_{CaS} = (\text{mass \% Ca}) \times (\text{mass \% S})$$

$$X_1 = e_S^{Ca}$$

$$X_2 = \log_{10}(K_{CaO})$$

$$X_3 = e_O^{Ca}$$

$$X_4 = \log_{10}(K_{CaS})$$

"i" will vary from 1 to 33 and "j" from 34 to 66.

Now, an objective function is defined, which is sum of squares of all the sixty-six functions, and is minimized by Genetic Adaptive Search technique. G.A. code provided by Carrol[31] has been used for this work.

Tables 4.10a and 4.10b provide the summary of G.A. parameters used and the optimized results using two sets of activity data (Rein and Chipman & Ohto and Suito).

It can be seen from the following table that interaction parameters and equilibrium constants determined by the two methods (G.A. and Mathematical model) compare closely with each other.

	G.A. Results		Mathematical model results	
	Rein & Chip.	Ohto & Suito	Rein & Chip.	Ohto & Suito
e_S^{Ca}	-29.34	-21.67	-29.0	-20.0
$Log_{10}(K_{CaO})$	-6.02	-5.07	-6.28	-5.54
e_O^{Ca}	-123.5	-92.91	-123.10	-89.34
$Log_{10}(K_{CaS})$	-3.96	-4.33	-4.91	-3.80

TABLE 4.1: Inclusion area fraction in Ladle and Tundish samples.

Heat Number	Ladle Sample	Tundish Sample
28585	0.16	0.11
28461	0.18	0.12
28463	0.165	0.098
26123	0.20	0.1
26785	0.17	0.13
26247	0.154	0.087
20564	0.149	-
28580	0.25	0.103
28588	0.14	0.095
28425	0.17	0.103
28440	0.129	0.105
28442	0.153	0.110
28503	0.109	0.109
28506	0.154	-
28666	0.135	0.11
28636	0.17	0.099
28638	0.13	-
28583	0.16	0.109
Minimum	0.109	0.087
Maximum	0.25	0.130
Average	0.15988	0.105

TABLE 4.2: Equilibrium constants and Interaction parameters used in the Thermodynamic model.

	Gaye & Gatellier [50]	Sigworth & Elliott [42]
$\log_{10}k_{Ca}$	1111111.1	221901.36
$\log_{10}k_{Al}$	8.3×10^{11}	9.515×10^{12}
$\log_{10}k_{Si}$	37354.6	37354.6
e_{Al}^{Al}	0.044	0.045
e_{Al}^{Si}	0.056	0.055
e_{Al}^{Ca}	- 0.072	- 0.047
e_{Al}^{O}	- 1.17	- 6.6
e_{Al}^{C}	0.091	0.043
e_{Al}^{S}	0.03	0.03
e_{Si}^{Si}	0.107	0.11
e_{Si}^{C}	0.018	0.078
e_{Si}^{Al}	0.058	0.058
e_{Si}^{Ca}	- 0.097	- 0.067
e_{Si}^{O}	- 0.14	- 0.23
e_{Si}^{S}	0.056	0.056
e_{O}^{Al}	- 1.98	- 3.91
e_{O}^{O}	- 0.17	- 0.176
e_{O}^{Ca}	- 310	- 62
e_{O}^{Si}	- 0.08	- 0.13
e_{O}^{C}	0.0	- 0.45
e_{O}^{S}	0.0	- 0.0642
e_{Ca}^{Al}	- 0.107	- 0.047
e_{Ca}^{Ca}	- 0.002	0.0
e_{Ca}^{Si}	- 0.138	- 0.138
e_{Ca}^{O}	- 780	- 389
e_{Ca}^{C}	0.0	- 0.097
e_{Ca}^{S}	0.0	0.0

TABLE 4.3: Slag Activity Data (1873 K)

H.No.	Mass,% CaO	^{a}CaO		mass,% SiO_2	$^{a}SiO_2$		mass,% Al_2O_3	$^{a}Al_2O_3$	
		Rein& Chipman	Ohto & Suito		Rein & Chipman	Ohto & Suito		Rein & Chipman	Ohto & Suito
29501	58.38	0.5	0.2	12.77	5.5×10^{-4}	5.5×10^{-4}	28.84	0.0625	0.06
29504	57.66	0.5	0.2	12.41	5.5×10^{-4}	5.5×10^{-4}	29.91	0.0625	0.07
29525	54.1	0.15	0.11	19	0.005	0.005	26.90	0.075	0.08
29530	53.45	0.15	0.11	19.11	0.005	0.005	27.43	0.075	0.1
29541	56.96	0.15	0.12	17.78	0.005	0.005	25.26	0.075	0.06
28636	41.91	0.04	0.15	19.0	0.010	0.01	19.06	0.24	0.25
28638	43.16	0.04	0.15	19.17	0.010	0.011	37.67	0.20	0.24
28666	49	0.16	0.1	16.93	0.005	0.005	34.6	0.14	0.17
29355	47.5	0.05	0.04	31.0	0.0375	0.0375	21.52	0.05	0.09
28442	47	0.12	0.07	20.68	7.5×10^{-3}	7.5×10^{-3}	32.32	0.14	0.15
28503	53.5	0.2	0.12	17.45	3.0×10^{-3}	3.0×10^{-3}	29.05	0.08	0.1
26061	52.1	0.035	0.04	35.74	0.05	0.05	12.16	0.04	0.028
26069	58.36	0.06	0.08	27.12	0.024	0.024	14.52	0.02	0.028
26073	59.46	0.05	0.08	25.55	0.02	0.02	14.99	0.025	0.028
26075	57.28	0.06	0.08	27.83	0.024	0.024	14.88	0.021	0.02
26097	58	0.13	0.12	18.71	7.5×10^{-3}	7.5×10^{-3}	23.3	0.075	0.05
26099	57.08	0.14	0.12	19.04	0.005	0.005	23.88	0.0625	0.05
26120	49.4	0.1	0.08	20.73	0.008	0.008	29.87	0.08	0.12
24595	48.3	0.035	0.04	35.42	0.0375	0.0375	16.28	0.017	6.5×10^{-3}
24598	51.53	0.035	0.05	33.40	0.04	0.04	15.07	0.018	0.029
24658	52.08	0.075	0.075	26.34	0.012	0.012	21.58	0.05	0.7
32590	53.12	0.35	0.15	12.19	1.0×10^{-3}	1.0×10^{-3}	33.98	0.070	0.13
32365	55.26	0.35	0.15	11.1	5.5×10^{-4}	5.5×10^{-4}	33.64	0.06	0.11
32389	49.94	0.15	0.1	17.81	3.0×10^{-3}	0.14	32.25	0.14	0.15
32391	46.57	0.1	0.085	17.87	0.005	0.0057	35.56	0.14	0.18
32308	53.23	0.4	0.15	11.42	5.5×10^{-4}	5.5×10^{-4}	35.34	0.06	0.15
33174	55	0.15	0.11	19.26	0.005	0.0057	25.76	0.0625	0.08
33216	44.29	0.1	0.1	14.54	3.0×10^{-3}	3.0×10^{-3}	41.16	0.15625	0.1
33214	52.22	0.1	0.085	22.0	7.5×10^{-3}	7.5×10^{-3}	25.74	0.0625	0.09
33226	45.87	0.11	0.1	14.94	3.0×10^{-3}	0.15	39.19	0.15	0.22
33185	53.0	0.075	0.075	24.94	7.5×10^{-3}	7.5×10^{-3}	22.18	0.05	0.07
33210	50.21	0.16	0.1	16.43	0.075	0.075	33.36	0.14	0.15
33238	60.42	0.15	0.21	16.75	0.005	0.07	22.83	0.07	0.045

TABLE 4.4: Comparison of calculated metal analysis by thermodynamic model.

	Calcium,mass%				Silicon,mass%				Aluminum,mass%			
	Sig.[5]		Gay[6]		Sig.		Gay		Sig.		Gay	
H.No	R/C[7]	O/S[8]	R/C	O/S	R/C	O/S	R/C	O/S	R/C	O/S	R/C	O/S
29501	0.0361	0.0141	0.3443	0.1372	0.0007	0.0007	0.0007	0.0007	0.0003	0.0003	0.0009	0.0009
29504	0.0113	0.0045	0.0235	0.0094	0.0019	0.0019	0.0019	0.0019	0.0006	0.0006	0.0019	0.0020
29525	0.0190	0.0139	0.3327	0.2442	0.0048	0.0048	0.0048	0.0048	0.0002	0.0003	0.0008	0.0008
29530	0.0086	0.0063	0.0663	0.0489	0.0074	0.0074	0.0075	0.0075	0.0003	0.0004	0.0011	0.0013
29541	0.0154	0.0123	0.2124	0.1693	0.0054	0.0054	0.0054	0.0054	0.0003	0.0002	0.0008	0.0008
28636	0.0044	0.0164	0.0727	0.2730	0.0102	0.0102	0.0102	0.0102	0.0005	0.0005	0.0015	0.0015
28638	0.0042	0.0157	0.0660	0.2489	0.0104	0.0104	0.0105	0.0104	0.0004	0.0005	0.0014	0.0015
28666	0.0044	0.0028	0.0122	0.0077	0.0141	0.0141	0.0142	0.0142	0.0007	0.0008	0.0024	0.0026
29355	0.0042	0.0034	0.0465	0.0376	0.0446	0.0466	0.0449	0.0449	0.0002	0.0003	0.0007	0.0010
28442	0.0119	0.0069	0.1416	0.0827	0.0085	0.0085	0.0085	0.0085	0.0004	0.0004	0.0012	0.0012
28503	0.0075	0.0045	0.0312	0.0188	0.0063	0.0063	0.0063	0.0063	0.0004	0.0005	0.0014	0.0016
26061	0.0033	0.0038	0.0413	0.0470	0.0558	0.0558	0.0562	0.0562	0.0002	0.0002	0.0006	0.0005
26069	0.0062	0.0083	0.0862	0.1154	0.0255	0.0255	0.0257	0.0257	0.0001	0.0002	0.0004	0.0005
26073	0.0015	0.0024	0.0044	0.0071	0.0521	0.0521	0.0524	0.0524	0.0003	0.0003	0.0010	0.0010
26075	0.0062	0.0083	0.0850	0.1133	0.0257	0.0256	0.0258	0.0258	0.0001	0.0001	0.0004	0.0004
26097	0.0065	0.0059	0.0347	0.0318	0.0130	0.0130	0.0131	0.0131	0.0004	0.0003	0.0012	0.0010
26099	0.0090	0.0077	0.0658	0.0562	0.0073	0.0073	0.0073	0.0073	0.0003	0.0003	0.0010	0.0008
26120	0.0080	0.0064	0.0740	0.0597	0.0102	0.0102	0.0103	0.0103	0.0003	0.0004	0.0010	0.0012
24595	0.0020	0.0022	0.0133	0.0151	0.0575	0.0575	0.0579	0.0579	0.0002	0.0001	0.0005	0.0003
24598	0.0014	0.0020	0.0059	0.0085	0.0803	0.0803	0.0810	0.0810	0.0002	0.0003	0.0007	0.0008
24658	0.0026	0.0026	0.0094	0.0103	0.0273	0.0273	0.0275	0.0275	0.0004	0.0014	0.0012	0.0046
32590	0.0298	0.0128	0.3336	0.1447	0.0012	0.0012	0.0012	0.0012	0.0003	0.0004	0.0009	0.0012
32365	0.0086	0.0037	0.0191	0.0083	0.0018	0.0018	0.0018	0.0018	0.0005	0.0007	0.0017	0.0024
32389	0.0027	0.0090	0.0041	7×10^{17}	0.0145	0.5870	0.0146	0.5967	0.0011	0.0011	0.0036	0.0037
32391	0.0024	0.0020	0.0053	0.0046	0.0167	0.0167	0.0168	0.0168	0.0008	0.0009	0.0027	0.0031
32308	0.0116	0.0044	0.0347	0.0133	0.0015	0.0015	0.0015	0.0015	0.0005	0.0007	0.0015	0.0024
33174	0.0039	0.0028	0.0097	0.0072	0.0151	0.0151	0.0152	0.0152	0.0005	0.0006	0.0017	0.0019
33216	0.0054	0.0054	0.0359	0.0355	0.0048	0.0048	0.0048	0.0048	0.0005	0.0004	0.0016	0.0013
33214	0.0239	0.0204	0.8433	0.7210	0.0054	0.0054	0.0054	0.0054	0.0002	0.0002	0.0006	0.0007
33226	0.0125	0.0119	0.1944	0.1870	0.0031	0.1481	0.0031	0.1491	0.0004	0.0004	0.0012	0.0014
33185	0.0020	0.0020	0.0055	0.0056	0.0211	0.0212	0.0214	0.0214	0.0004	0.0005	0.0014	0.0017
33210	0.0135	0.0084	0.1447	0.0906	0.0900	0.0900	0.0904	0.0904	0.0004	0.0004	0.0013	0.0013
33238	0.0040	0.0060	0.0108	0.0160	0.0144	0.0192	0.0144	0.1985	0.0005	0.0004	0.0017	0.0013

[5] Elliott and Sigworth
[6] Gaye and Gatellier
[7] Rein and Chipman
[8] Ohto and Suito

TABLE 4.5: O.L.P. Chemical analysis(%) and Temperature(°C)

H. No.	C	S	Si	Al	O_2	Temp
24587	0.06	0.018	0.020	0.012	0.0127	1660
24595	0.05	0.018	0.022	0.007	0.0097	1670
24598	0.05	0.018	0.028	0.005	0.0086	1670
24600	0.05	0.015	0.020	0.012	0.0070	1660
24603	0.06	0.16	0.016	0.009	0.0050	1670
24648	0.05	0.017	0.014	0.011	0.0193	1670
24653	0.04	0.020	0.018	0.006	0.0225	1670
24655	0.07	0.026	0.010	0.006	0.0135	1670
24657	0.06	0.019	0.018	0.006	0.0212	1656
24658	0.06	0.0.23	0.018	0.006	0.0085	1670
24660	0.05	0.024	0.018	0.006	0.0100	1670
24675	0.05	0.020	0.020	0.006	0.0157	1670
24677	0.05	0.020	0.020	0.014	0.0161	1650
24685	0.06	0.020	0.015	0.007	0.0120	1670
24694	0.05	0.027	0.023	0.007	0.0104	1670
24724	0.06	0.020	0.023	0.005	0.0146	1660
26021	0.05	0.018	0.023	0.018	0.0096	1670
26028	0.04	0.019	0.022	0.014	0.0070	1645
26033	0.05	0.021	0.019	0.007	0.0117	1640
26061	0.05	0.017	0.016	0.007	0.0110	1660
26069	0.05	0.018	0.017	0.013	0.0148	1670
26103	0.05	0.018	0.025	0.005	0.0160	1650
26073	0.05	0.018	0.012	0.008	0.0100	1670
26075	0.05	0.021	0.012	0.009	0.0096	1670
26097	0.6	0.018	0.007	0.011	0.0180	1650
26099	0.05	0.019	0.018	0.009	0.0113	1670
26101	0.05	0.020	0.021	0.009	0.0133	1670
26120	0.05	0.018	0.010	0.008	0.0110	1670
26123	0.05	0.022	0.023	0.010	0.0110	1655
26228	0.04	0.020	0.032	0.008	0.0113	1670
26239	0.04	0.015	0.020	0.006	0.0160	1670
26242	0.05	0.017	0.028	0.008	0.0104	1670
					Average	1665

TABLE 4.6: Actual chemical analysis of EWNR (mass %)

H.No.	C	Mn	S	Si	Ca	Al	O_2[9]
29501	0.05	0.53	0.021	0.018	0.0036	0.005	0.004507
29504	0.05	0.52	0.019	0.020	0.0035	0.004	0.002737
29525	0.05	0.49	0.017	0.023	0.0042	0.005	0.005240
29530	0.04	0.50	0.018	0.020	0.0035	0.005	0.004223
29541	0.05	0.46	0.020	0.021	0.0025	0.006	0.004960
28636	0.04	0.52	0.018	0.017	0.0041	0.004	0.005098
28638	0.04	0.50	0.018	0.014	0.0070	0.010	0.005041
28666	0.05	0.53	0.017	0.028	0.0047	0.006	0.003057
29355	0.05	0.48	0.029	0.026	0.0028	0.006	0.004693
28442	0.06	0.49	0.016	0.014	0.0047	0.005	0.004837
28503	0.05	0.51	0.027	0.018	0.0039	0.007	0.003546
26061	0.05	0.53	0.014	0.018	0.0063	0.006	0.004842
26069	0.05	0.50	0.017	0.022	0.0029	0.006	0.004976
26073	0.05	0.49	0.014	0.014	0.0027	0.005	0.003170
26075	0.05	0.46	0.015	0.018	0.0039	0.005	0.004967
26097	0.06	0.51	0.018	0.021	0.0055	0.007	0.003897
26099	0.06	0.52	0.018	0.018	0.0050	0.006	0.004265
26120	0.06	0.50	0.016	0.023	0.0050	0.007	0.004550
24595	0.05	0.56	0.015	0.020	0.0049	0.006	0.004128
24598	0.05	0.50	0.016	0.020	0.0047	0.010	0.003598
24658	0.05	0.53	0.018	0.014	0.0035	0.006	0.003400
32590	0.05	0.47	0.015	0.021	0.0039	0.005	0.004713
32365	0.06	0.49	0.018	0.014	0.0027	0.002	0.002839
32389	0.05	0.48	0.024	0.022	0.0037	0.006	0.002335
32391	0.05	0.49	0.018	0.023	0.0064	0.007	0.002807
32308	0.05	0.46	0.017	0.022	0.0021	0.005	0.003158
33174	0.05	0.52	0.024	0.016	0.0020	0.002	0.002957
33216	0.05	0.55	0.018	0.025	0.0050	0.005	0.004089
33214	0.05	0.48	0.015	0.028	0.0023	0.005	0.006064
33226	0.05	0.48	0.012	0.019	0.0070	0.006	0.005090
33185	0.04	0.54	0.020	0.025	0.0026	0.006	0.003052
33210	0.05	0.43	0.016	0.028	0.0059	0.007	0.004653
33238	0.05	0.52	0.015	0.020	0.0024	0.005	0.003031

[9] dissolved Oxygen

TABLE 4.7a: Output of Regression analysis with different chosen values of e_S^{Ca}

Slag Activity by: Rein & Chipman [10]

e_S^{Ca}	Correlation Co-efficient	Regression Coefficient (e_O^{Ca})	Standard Error of Coefficient	Regression Constant (-log10(K_{CaO}))	Standard Error of Constant
-20.0	0.739	-111.94	19.94	6.01	0.282
-23.0	0.740	-119.66	19.50	6.10	0.285
-26.0	0.741	-121.38	19.72	6.19	0.292
-29.0	0.743	-123.10	19.96	6.28	0.292
-32.0	0.742	-124.82	20.22	6.37	0.295
-35.0	0.742	-126.54	20.49	6.46	0.300
-38.0	0.742	-128.26	21.78	6.56	0.303
-41.0	0.742	-129.98	21.09	6.65	0.308
-44.0	0.741	-131.70	21.41	6.74	0.313
-47.0	0.740	-133.43	21.74	6.83	0.318

TABLE 4.7b: Output of Regression analysis with different chosen values of e_S^{Ca}

Slag Activity by: Ohto & Suito [27]

e_S^{Ca}	Correlation Co-efficient	Regression Coefficient (e_O^{Ca})	Standard Error of Coefficient	Regression Constant (-log10(K_{CaO}))	Standard Error of Constant
-5.0	0.765	-80.743	12.22	5.08	0.18
-8.0	0.768	-82.46	12.34	5.17	0.18
-11.0	0.771	-84.18	12.49	5.26	0.18
-14.0	0.773	-85.90	12.67	5.35	0.18
-17.0	0.773	-87.62	12.89	5.44	0.19
-20.0	0.774	-89.34	13.12	5.54	0.19
-23.0	0.773	-91.06	13.39	5.63	0.19
-26.0	0.773	-92.78	13.68	5.72	0.20
-29.0	0.771	-94.50	13.99	5.81	0.20

TABLE 4.8: Summarized output of Linear Regression

	Rein & Chipman	Ohto & Suito
e_S^{Ca}	-29.0	-20.0
Correlation Coefficient	0.743	0.774
Regression Coefficient = e_O^{Ca}	-123.10	-89.34
Standard Error of Coefficient	19.96	13.12
Regression Constant = -log10(K_{CaO})	6.28	5.54
Standard Error of Constant	0.29	0.19

TABLE 4.9: Inclusion Spot Analysis Result

Heat Number		26785	28503	29530
Inclusion	CaO, mass %[10]	45.92	56.97	54.53
	SiO_2, mass %	24.27	16.40	20.75
	Al_2O_3, mass %	29.80	26.62	24.72
	^{a}CaO	0.035	0.2	0.15
	$^{a}SiO_2$	0.0375	0.003	0.005
	$^{a}Al_2O_3$	0.0625	0.0625	0.0625
Slag	CaO, mass %	49.86	53.49	53.45
	SiO_2, mass %	33.11	17.45	27.43
	Al_2O_3, mass %	17.03	29.05	19.11
	^{a}CaO	0.035	0.2	0.15
	$^{a}SiO_2$	0.0375	0.003	0.005
	$^{a}Al_2O_3$	0.030	0.08	0.075

[10] mass %s are the normalized values

TABLE 4.10a: List of G.A. Inputs

		Rein & Chipman	Ohto & Suito
Population Size		50	50
Mutation Probability		0.0004	0.0003
Cross-Over Probability		0.85	0.90
Maximum Generation		1000	1000
Minimum Value	X1 (e_S^{Ca})	-38.0	-25.0
	X2 ($\log_{10}(K_{CaO})$)	-7.5	-6.5
	X3 (e_O^{Ca})	-128.0	-100.0
	X4 ($\log_{10}(K_{CaS})$)	-7.0	-6.0
Maximum Value	X1	-30.0	-15.0
	X2	-5.5	-4.5
	X3	-120.0	-80.0
	X4	-3.0	-4.0

TABLE 4.10b: G. A. Result

	Rein & Chipman	Ohto & Suito
e_S^{Ca}	-34.17	-21.67
$\log_{10}(K_{CaO})$	-6.58	-5.07
e_O^{Ca}	-124.94	-92.91
$\log_{10}(K_{CaS})$	-3.22	-4.33
No.of Generations For convergence	457	60

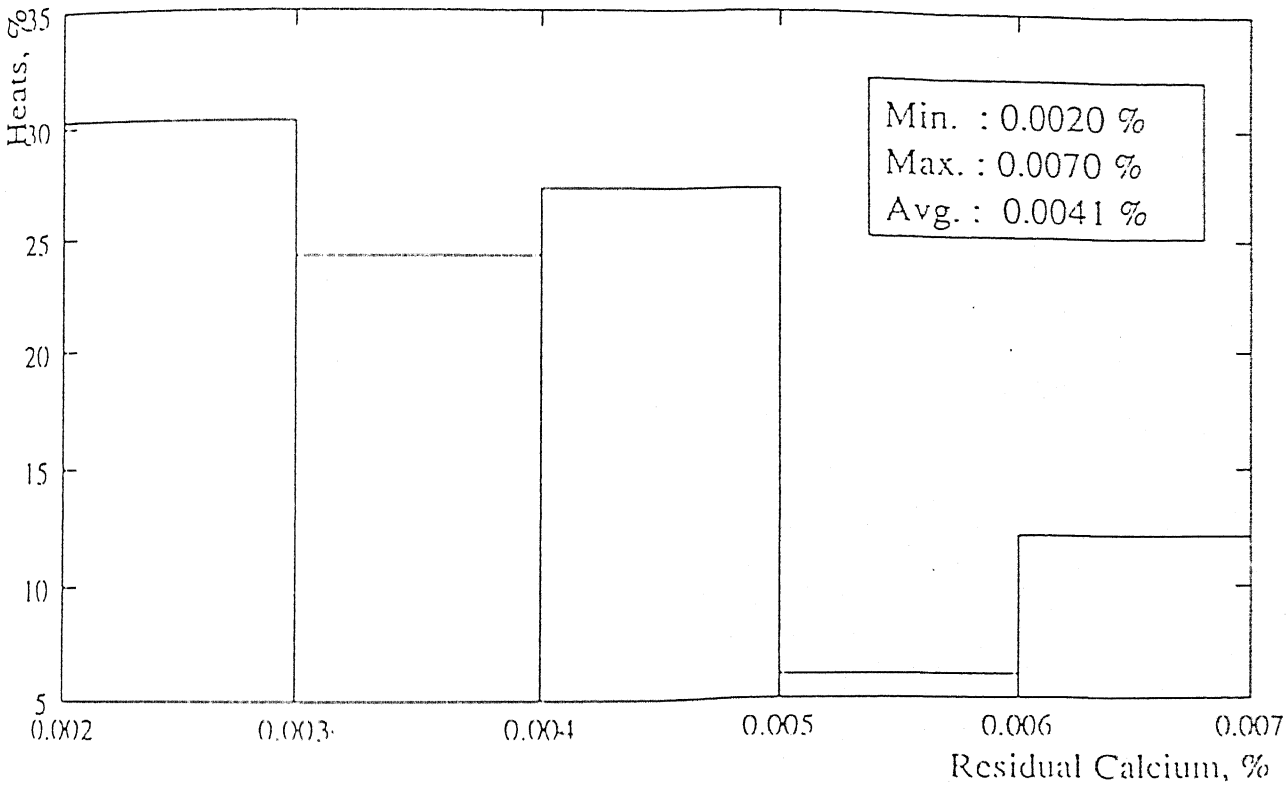

Figure 4.1: Frequency distribution of residual calcium in EWNR steels.

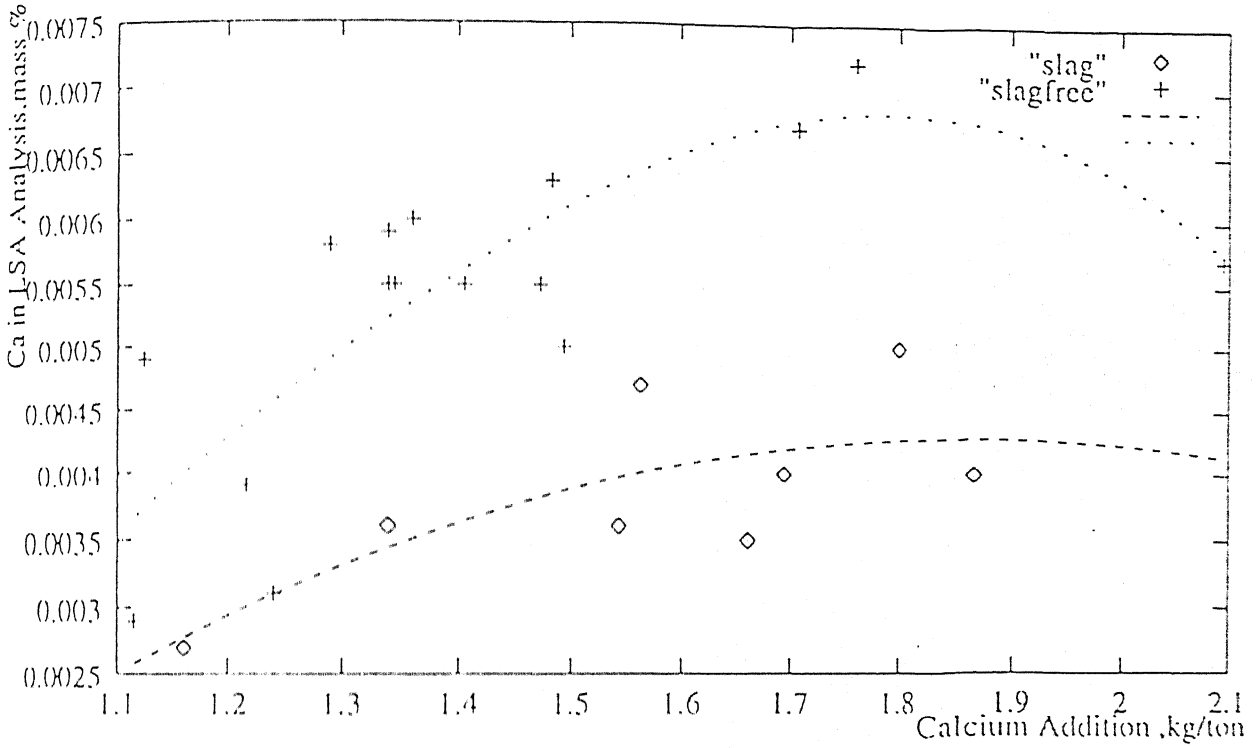

Figure 4.2: Effect of slag carry over on calcium recovery.

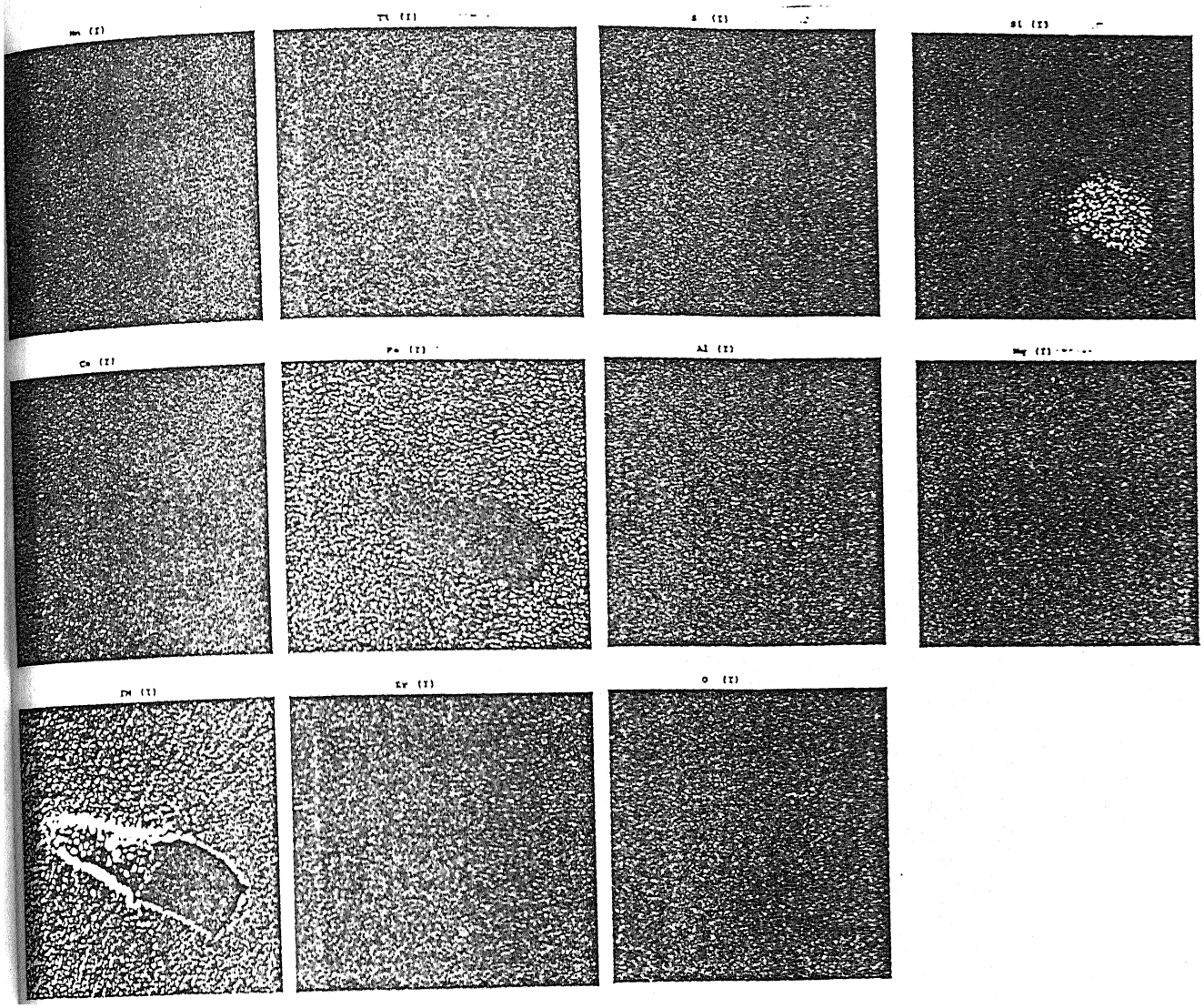

Figure 4.3: Typical FeO - SiO_2 inclusion observed in EWNR.

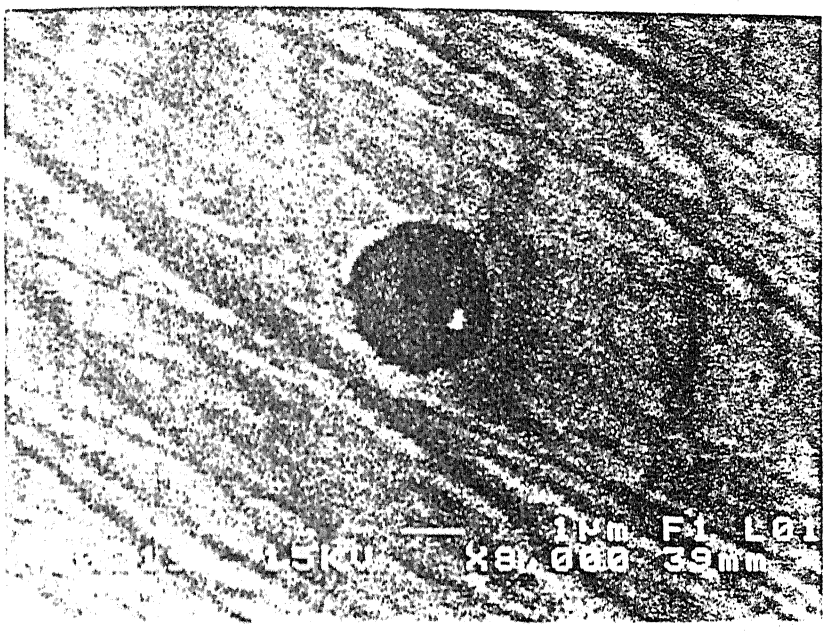

Figure 4.4: Typical complex oxide inclusion observed in EWNR.

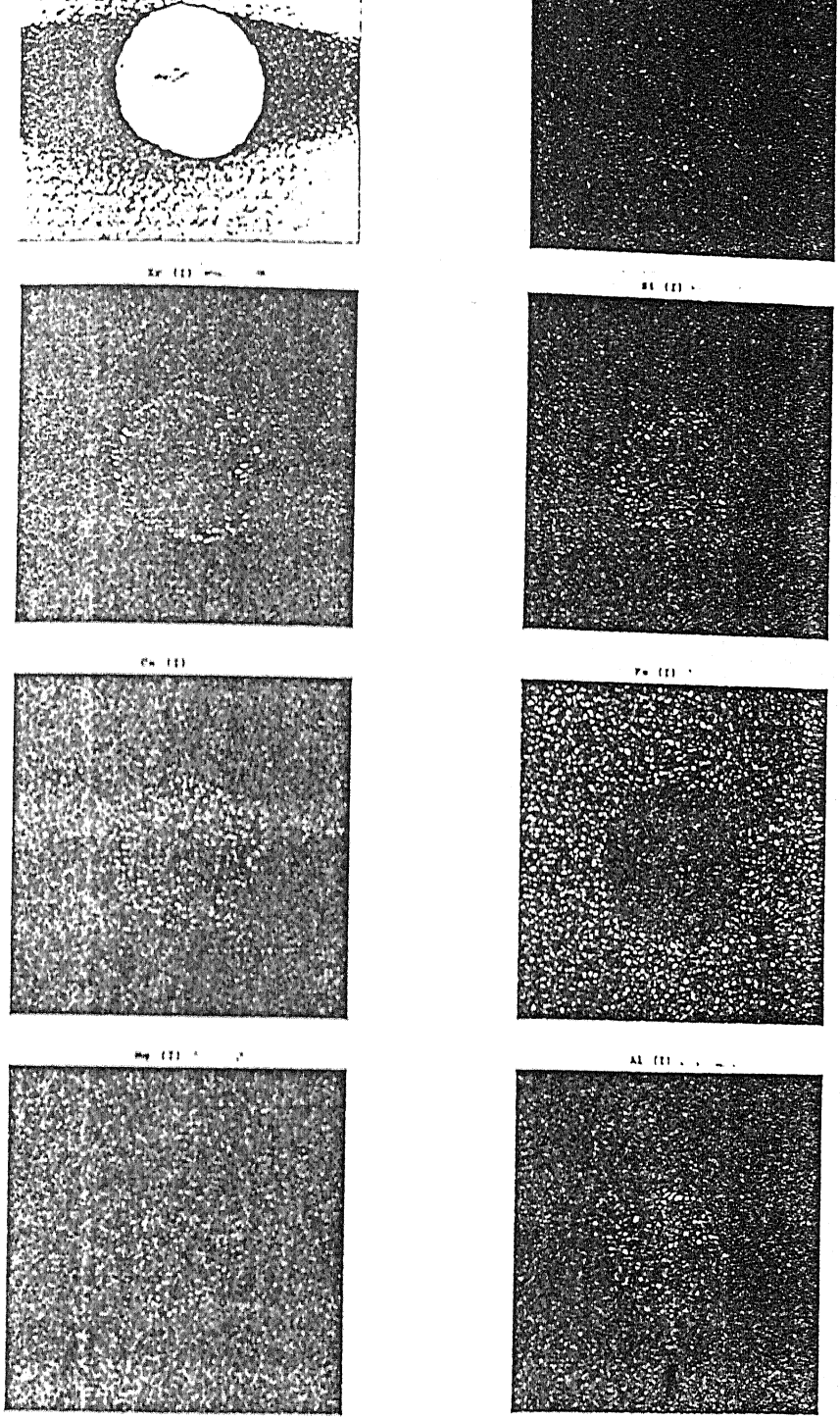

Figure 4.5: Typical complex oxide inclusion with thin CaS layer.

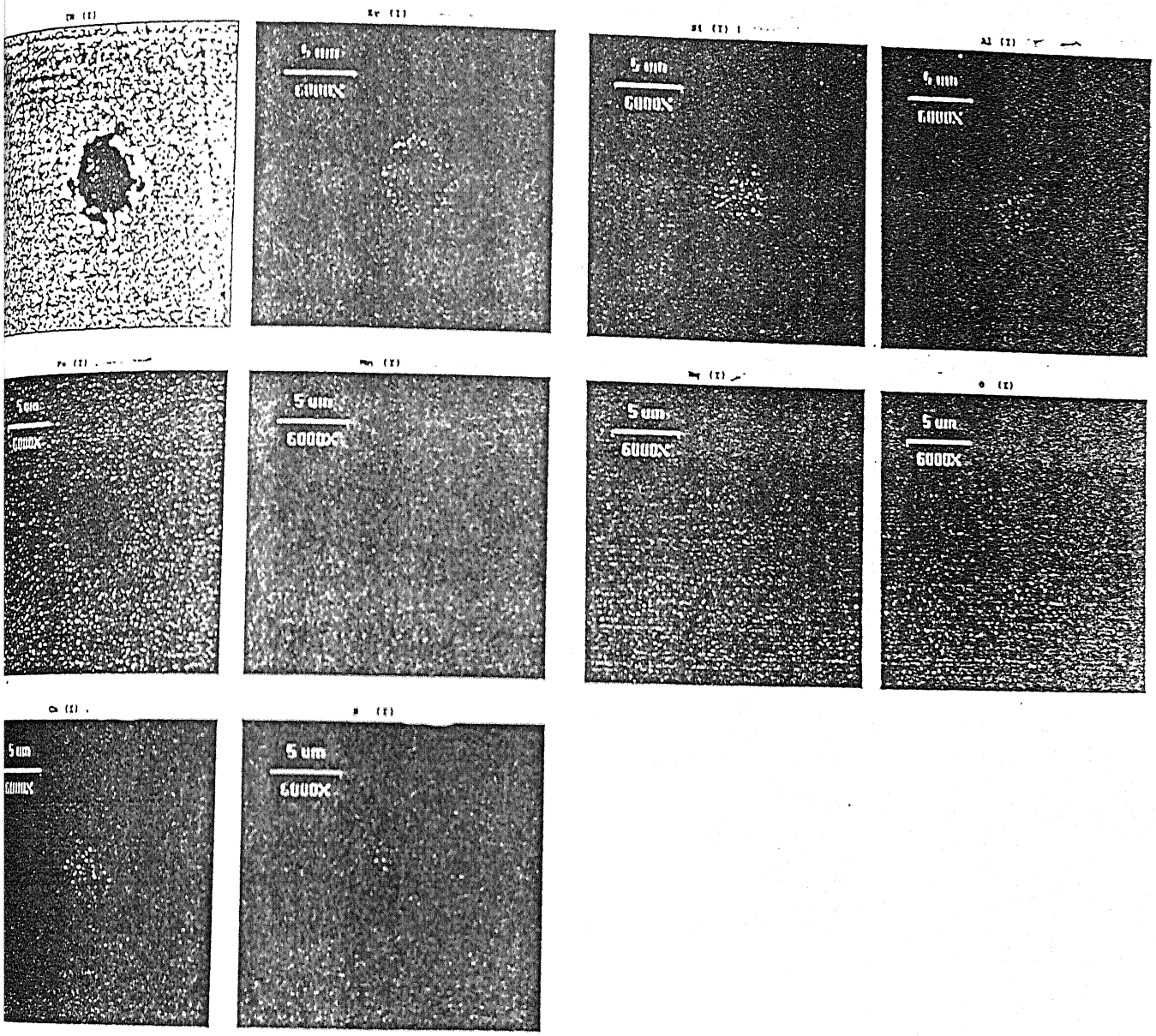

Figure 4.6: Typical complex oxide inclusion with thick CaS layer.

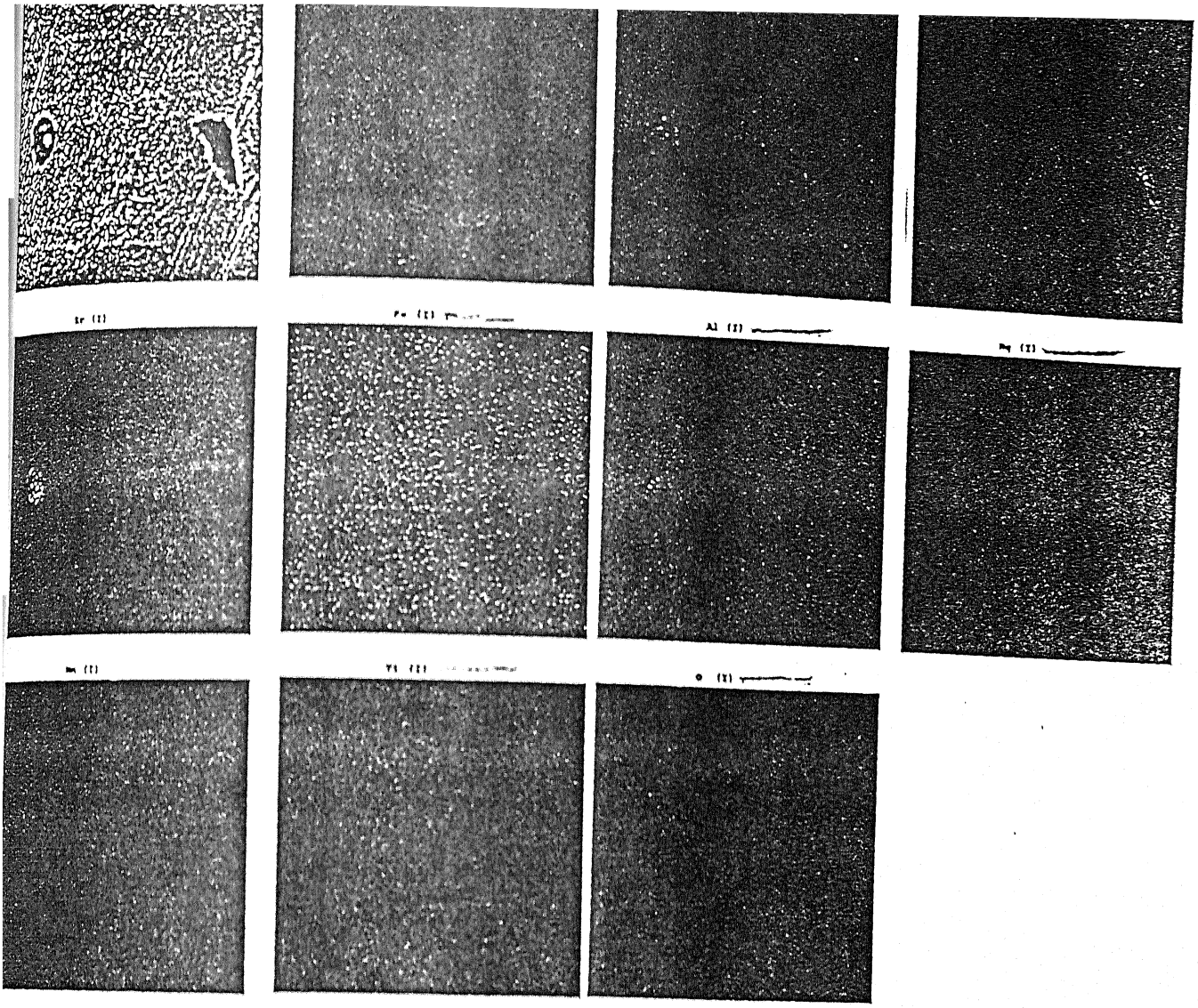

Figure 4.7: Typical complex oxide inclusion with uniformly distributed sulphur within the inclusion matrix.

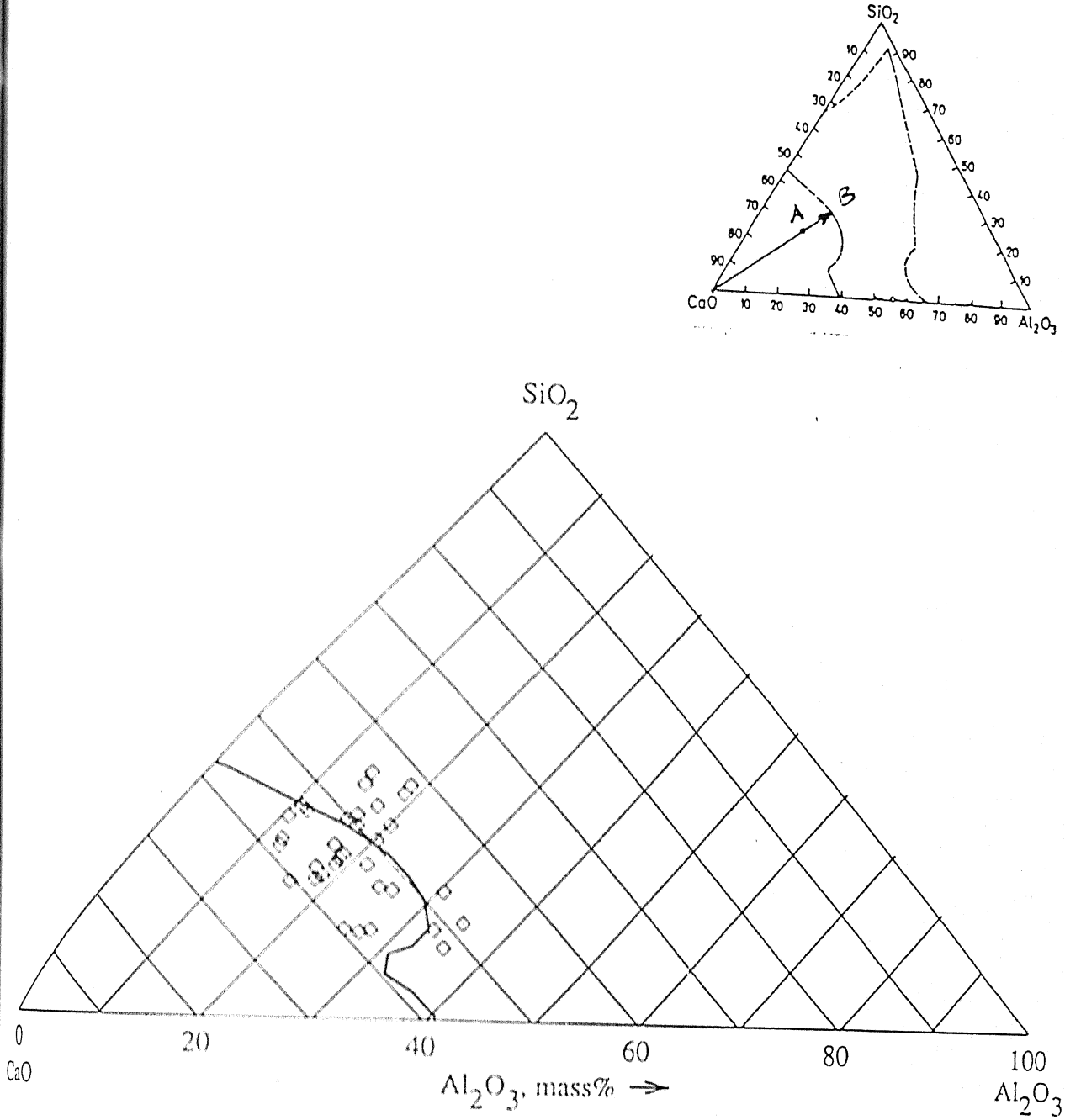

Figure 4.8: After injection treatment slag composition plot.

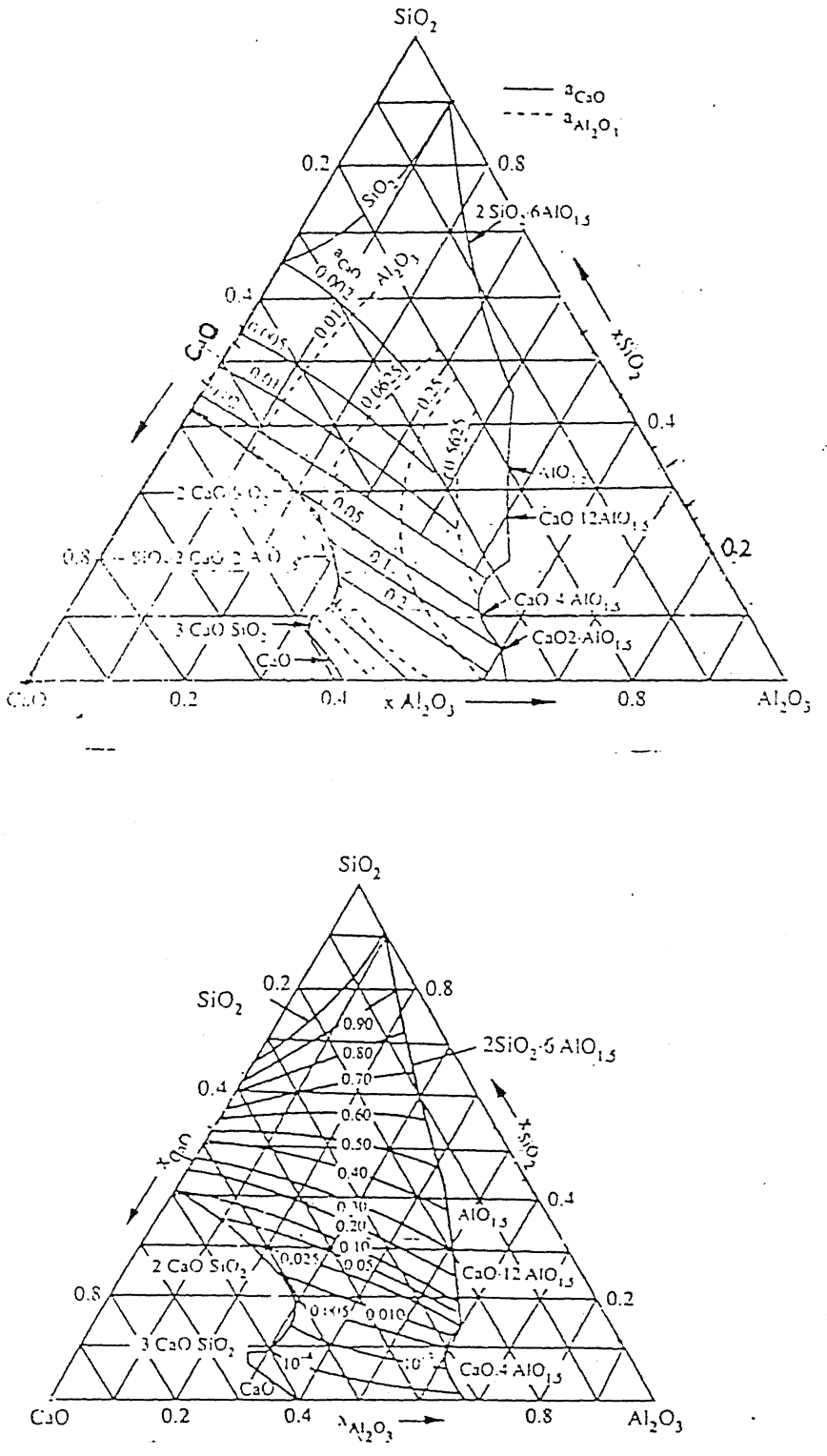

Figure 4.9 a: Iso-activity ternary diagram by Rein and Chipman.

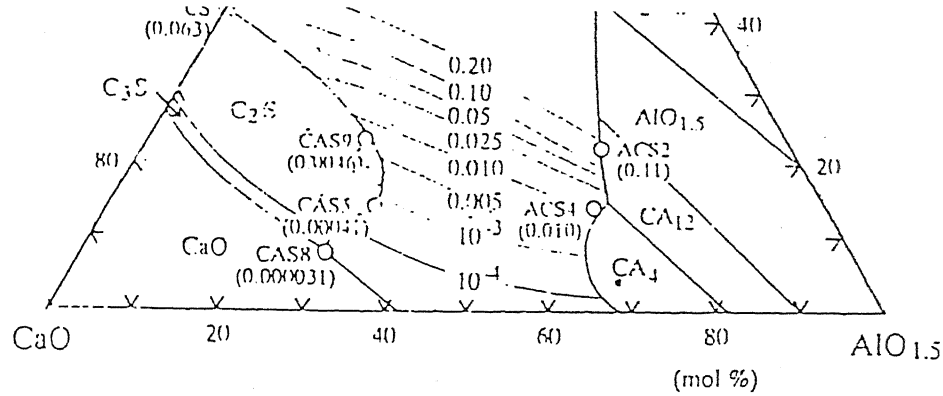

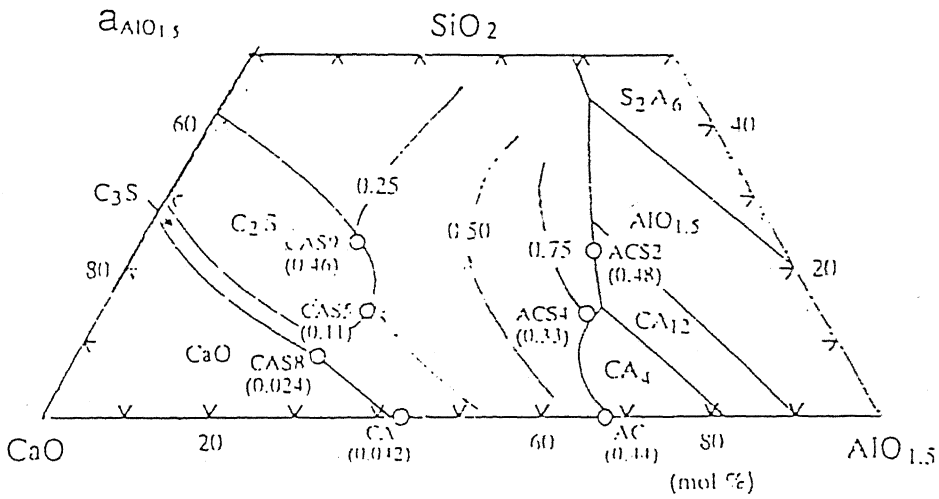

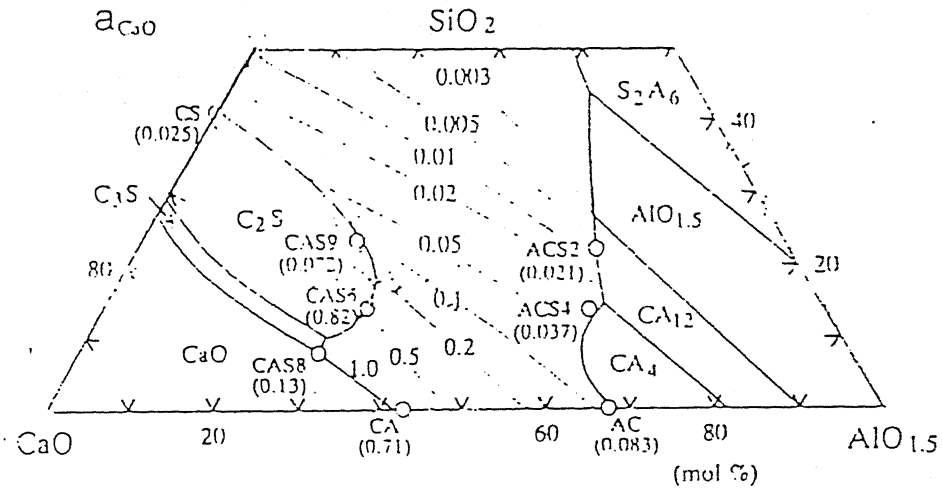

Figure 4.9 b: Iso-activity ternary diagram by Ohto and Suito.

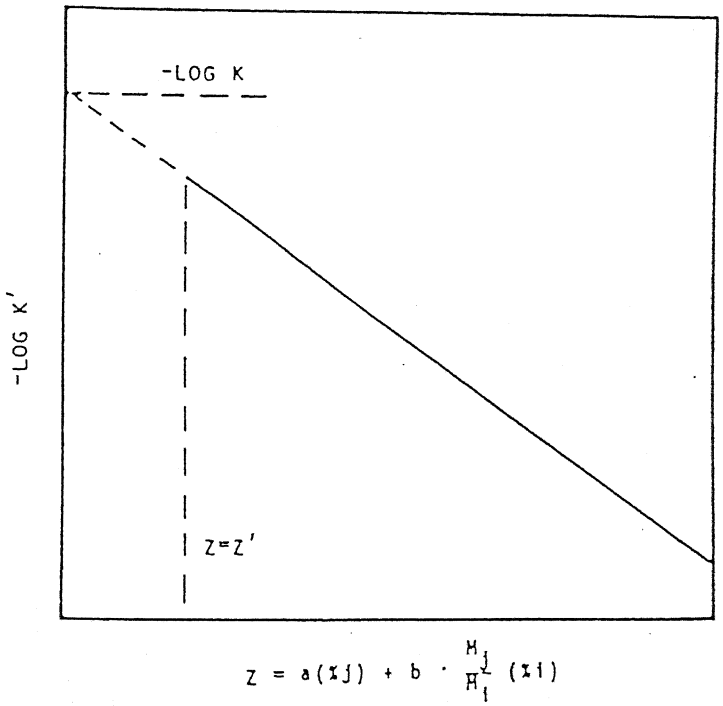

Figure 4.10: Plot between - log $_{10}$ k' and composition co-ordinate (z)

ANALYSIS CONDITIONS

Quant. Method	: XPP/ASAP
Acquire Time	: 40 secs
Normalization Factor	: 100.00

Element	Line	Weight%	K-Ratio	Cnts/s	Atomic%
Mg	Ka	3.67	0.0255	41.29	5.96
Al	Ka	19.83	0.1524	280.99	29.00
Si	Ka	12.18	0.0922	175.27	17.12
S	Ka	4.93	0.0376	62.32	6.06
Ca	Ka	23.69	0.2195	242.74	23.32
Fe	Ka	11.36	0.1032	43.88	8.03
Zr	La	24.34	0.1750	127.89	10.53
Total		100.00			

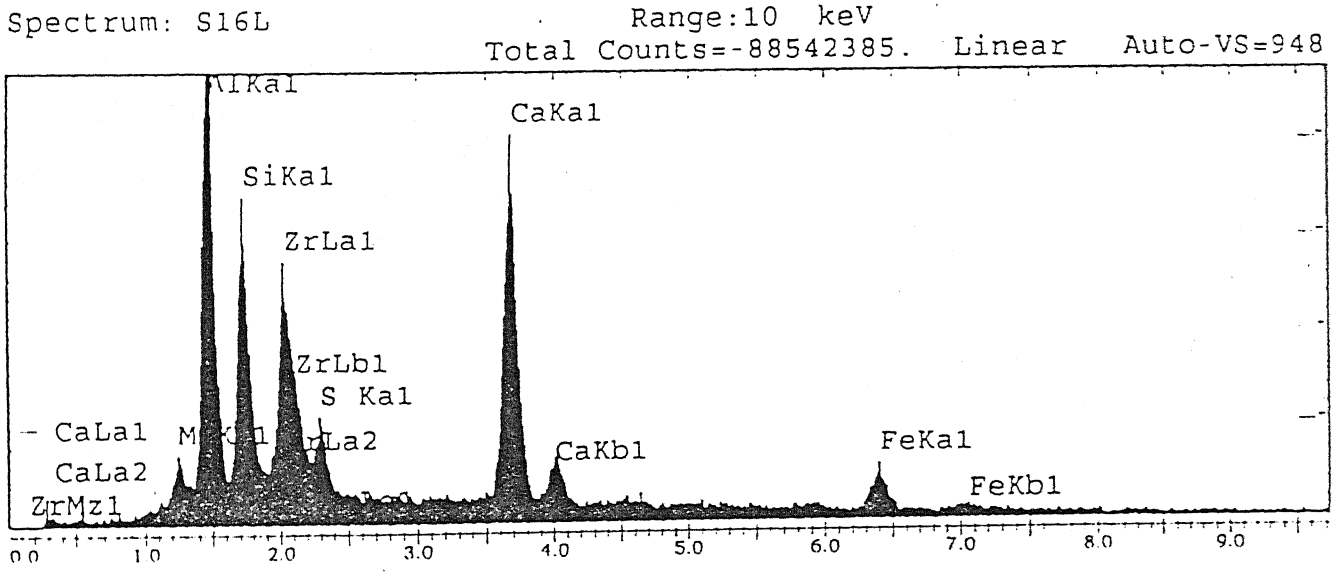

Figure 4.11: Spot analysis of a typical inclusion found in H.No.26785

ANALYSIS CONDITIONS

Quant. Method	: XPP/ASAP
Acquire Time	: 40 secs
Normalization Factor	: 100.00

Element	Line	Weight%	K-Ratio	Cnts/s	Atomic%
Al	Ka	11.71	0.0735	135.99	20.73
Si	Ka	3.61	0.0256	48.77	6.14
S	Ka	1.94	0.0158	26.27	2.89
Ca	Ka	14.47	0.1441	159.90	17.25
Fe	Ka	51.88	0.4962	211.75	44.39
Zr	La	16.39	0.1205	88.35	8.59
Total		100.00			

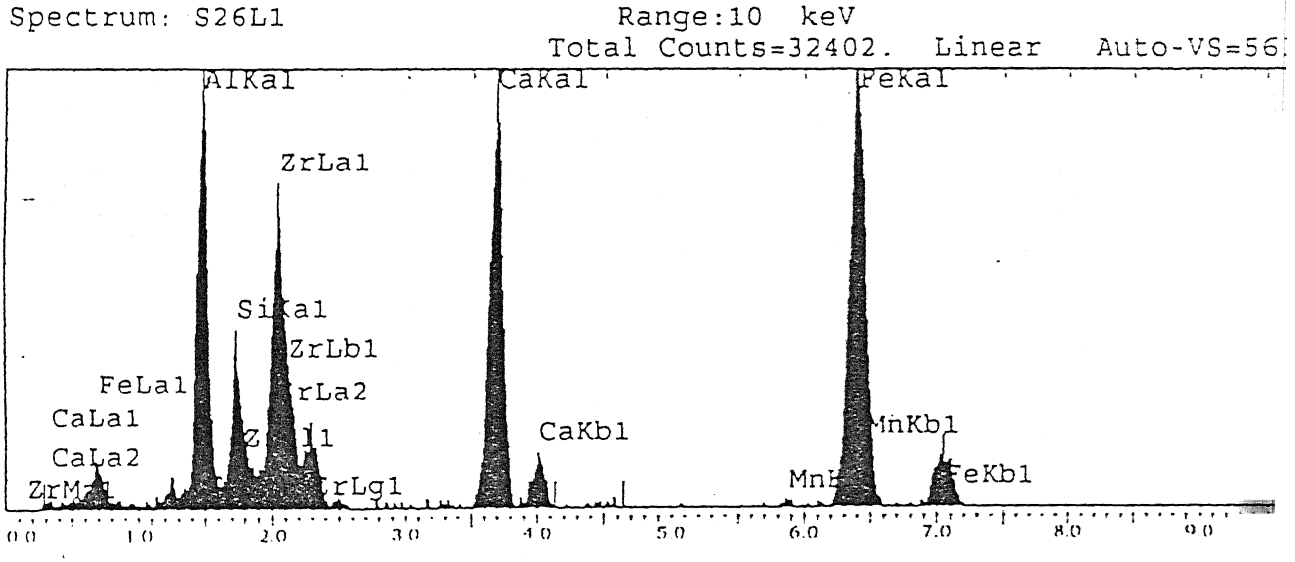

Figure 4.12: Spot analysis of a typical inclusion found in H.No.28503

ANALYSIS CONDITIONS

Quant. Method	: XPP/ASAP
Acquire Time	: 41 secs
Normalization Factor	: 100.00

Element	Line	Weight%	K-Ratio	Cnts/s	Atomic%
Mg	Ka	3.93	0.0301	49.72	5.09
Al	Ka	37.76	0.3037	571.85	44.01
Si	Ka	15.85	0.1046	202.91	17.75
Ca	Ka	41.65	0.3843	433.88	32.69
Fe	Ka	0.81	0.0069	2.98	0.46
Total		100.00			

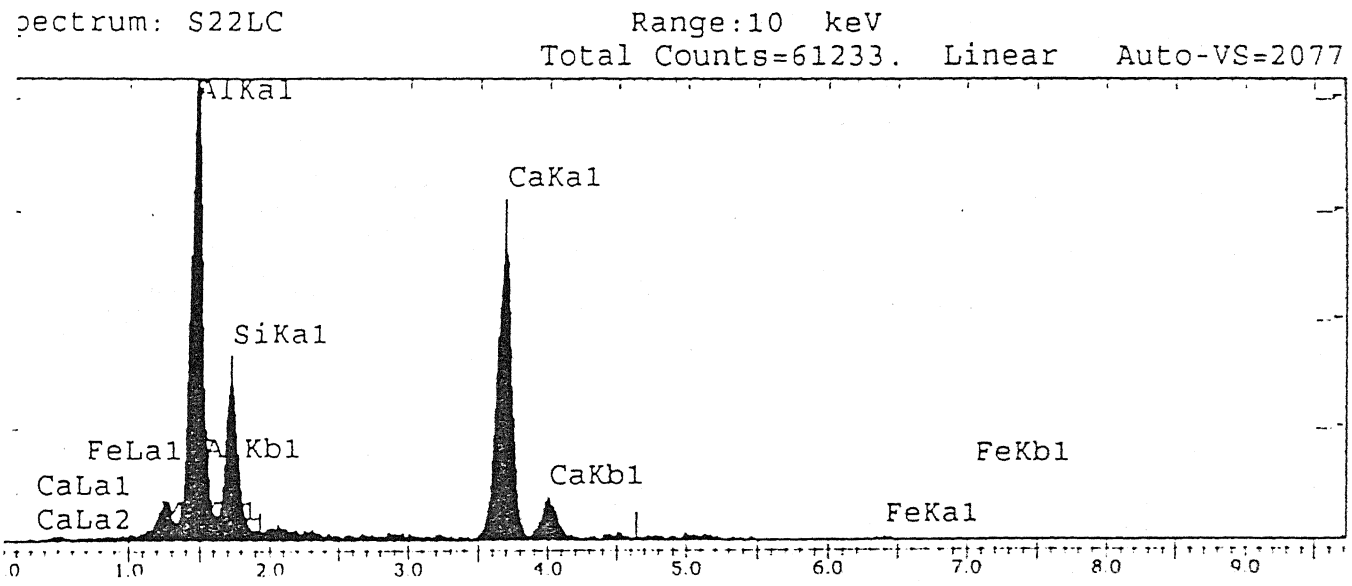

Figure 4.13: Spot analysis of a typical inclusion found in H.No.29530

CHAPTER 5

CONCLUSIONS AND SUGGESTIONS FOR FUTURE WORK

5.1 Conclusions

Closeness of activity values of CaO, SiO_2 and Al_2O_3 found from the slag composition and inclusion spot analysis (Table 4.9) indicates the existence of thermodynamic equilibrium between metal, slag and inclusions. Study of the inclusions revealed that the major part of reported calcium mass percentage (by optical spectroscope) is present in the dissolved state. Also, product analysis of various casts of EWNR steel indicates that there is a difference of at least 0.003 % between the aluminum (mass %) achieved and the upper limit of specified analysis (Table 1.1). Thus it can be suggested that the aluminum content of steel may be slightly increased without causing an adverse effect on the castability of the grade. An increase in the amount of aluminum should help in achieving a relatively lower dissolved oxygen level before injection and this in turn should result in improved recovery of calcium. Now, keeping the scope of increasing aluminum concentration in steel in mind use of Ca-Fe-Al wire instead of calcium – iron (CaFe) wire can prove advantageous because this will lead to both increase in aluminum concentration of steel and improved recovery of calcium because complex deoxidant is known to result in enhanced deoxidation efficiency.

SEM analysis of ladle samples indicated to contain high concentration of silicate inclusions. Use of top slag (having a low activity of SiO_2) to absorb these inclusions would considerably improve the cleanliness of steel and would also provide an opportunity to increase the silicon content of steel because reported silicon mass percentage in the steel sample (by optical microscope) includes the silicon present in $FeO\text{-}SiO_2$ inclusions. Use of top slag will also help in the prevention of the reoxidation of steel during purging operation. Figure 4.2 emphasizes the need of preventing converter's slag from getting carried over in to the ladle from both improved cleanliness of the steel melt and recovery suggested enhancement point of view.

5.2 Suggestions for future work

1. Modification of both oxides and sulphide inclusions may be studied by frequent sampling during and after Calcium injection in to steel.
2. Detailed S.E.M. investigation of deposited sample on the tundish nozzle will provide better understanding of factors causing tundish nozzle clogging.
3. Heat and Mass balance calculations should be performed to find out means for improving Calcium yield.

Reference Table:

1.F.D.Richardson, J.H.E.Jeffers: *Journal of Iron and Steel Institute*, 1948, No.160, p 261.

2.E.Schurmann, P.Funders, H.Litterscheidt: *Arch. Eisenhuttenw*, 1975, No. 46, p.473.

3.E.Forster, W.Klapdar, H.Richeter,H.W.Rommerswinkel, E. Spetzler, and J. Wendroff: *Stahl und Eisen*, 1974, vol.94, p.474.

4.J.G.Kaiser: *American magazine*, June 30, 1983, No.33.

5. E. T. Turkdogan: *Steel Research*, vol.62, 1991, No.9, p379.

6.Stefan Gustaffson & P. O. Mellberg: *Scand. J. Met.* 1980, vol.9, p.111-116.

7.J.F.Elliott, M.Glieser & V.Rama Krishna: *Thermo-chemistry for Steel Making*, 1963, Vol.2, p.304-462.

8.V.Presern, B.Korousic, J.W.Hastle: *Steel Research*, vol.62, 1991, No.7, p.289-295.

9.A.Muan, E.F.Osbom: *Phase equilibria among oxides in steel making*, Addison - wesley, 1965, p.95.

10.R.H.Rein and J.Chipman: *Trans. Metall. Soc. AIME*, vol.233, 1965.

11.Ototani, Katanra, Degawa: *Tetsu to Hagane*, vol.61, 1975, p.2167.

12.D.L.Sponsoller, R.A.Flinn: *Trans. AIME*, 1964, vol.230, p.876-888.

13.Oyama, Tanaka, Kitammra: *Tetsu to Hagane*, vol.63, 1977, p.159.

14.Takenouchi, Suzuki: *Tetsu to Hagane*, vol.63, 1977, p.1653.

15.Hirahara, Murukawa, Yamazaki, Takahashi, Shiroda: *Tetsu to Hagane*, vol.64, 1978, p.121.

16.Umeda, Ikeda, Kawai, Sugisawa: *Tetsu to Hagane*, vol. 65, 1979, p.29.

17. E.T.Turkdogan: *Proc. Third Int. conf. molten slags and fluids*, University of Strathclyde, Glascow, 1988.

18.M.F.Riley, L.G.Nusselt: *Fifth international Iron & Steel congress*, 1986, p.177-182.

19. V.Presern: *The sixth International Iron & Steel congress*, Nagoya, vol.3, 1990, p.520.

20.H.Gaye, P.V.Ribond, J.Welfringer: IRSID, *Marizierer-les-Metz*, France.

21. G.M.Faulring: *Electric furnace conference proceedings*, 1988, p.89-96.

22.H.Pielet & D.Bhattacharya: *Met. Transaction 'B'*, vol.15 B, Sept.1984, p.547-561.

23.J.W.Farrell, D.C.Hilty: *Electric furnace conference proceedings*, 1971, No.32, p.31-46.

24.Asit Roy, R. Dutta, P. K. Mukhopadhyay, A. Chatterjee: *TATA Search*, 1995, p.94-98.

25.F.Pellicani, B.durand, A.Guessier: *Proceedings of the first international Calcium treatment symposium*, June 30, Glascow, 1988, p.15.

26.John M.Svoboda: Electrical furnace proceedings, 1987, p.243-263.

27.Hiroki Ohta, HIkeaki Suito: *Metallurgical and Materials transaction*, 415 'B', Vol.27'B', 1996, p.943-953.

28.C.H.P.Lupis: *Acta Met*, 1968, No.16, p.1365-1375.

29.Davidf E.Goldberg: *Genetic algorithms in search optimization and machine learning*, Addison – wesley publishing company, Inc., 1953.

30.Kalyanmoy deb: *Optimization for engineering design – Algorithms and examples*, Prentice hall of India pvt. Ltd., New Delhi, 1995.

31.Carroll's G. A. Code: *http://www.staff.nine.edu/~carroll/ga.html*

32.S.Kobyashi et al.: *Tetsu to Hagane*, vol. 56, 1970, No.8, p.998-1013.

33.K.Suzuki, et al.: *Tetgn to Hagane*, vol.63, 1977, No.11, p.585.

34.Q.Han et al.: *Metallurgical Transactions*, vol. 19 B, 1988, p.617-612.

35.S.Gustafsson, et al.: *Thermodynamic Behavior of Calcium in liquid iron, Final Report*, ECSC, Nov.1982.

36.M.Nadif, C. Gatellier,: *Rev. Met.*, CIT 83, 1986, No. 5, p.377-394.

37.A.K.Bagaria, Brahma Deo, A.Ghosh: *International symposium on modern developments in steel making*, Jsr. (INDIA)

38. I.M.Mihanher, Izn. Vuzov: *Chernaya Metallurgia*, 1981, Vol. 8, p.1-4.

39.O.Haida, T.Emi, K.Sanbongi, T.Shiraighi, A.Fuzinara: *Transactions of Iron and Steel Institute*, 1971, vol.11, p.260-269.

40.F.Rayes-Carmona, A.Mitchell, E.Samuelsson, *Trans. ISIJ*, 1984, 24, p.585-588.

41. Hiroyasu Itoh, Mitsntaka Hino and Shiro Ban-Ya, *Met.and Materials transaction B*, Vol.28B, October 1997,p953-955.

42.G.K.Sigworth, J.F.Elliott: *Met. Science.*, 1974, vol.8, p.298-310.

43.Takashi Kimura, Hideaki Suito: *Metallurgical and Materials Transactions 'B'*, vol. 25 B, Feb.1994, p.33-42.

44.Sung-Wook CHO and HIdenki Suito: *ISIJ International*, vol.34, 1994, NO.3, p.265-269.

45.C.Gatellier, M.Olette: *Rev. Metall.*, Cah. Inf.Tech, June 1979, 377-386.

46.D.Janke, W.A.Fisher: *Arch. Eisenhuttenwesen*, vol.47, 1976, p195-197.

47.Suzuki, K. : *Tetsu to Hagane*, 1977, vol.63, p.585.

48.Pergfei Wang and Q.Han: *Acta metallurgia sinica*, 1988, vol.24 B, no. 1, p.7-11.

49. A.Palmers, J.Defays & L.Philippe, *CRM No.55*, Nov.,1979, p.15-23.

50.M.Joyant, C.Gatellier: *Report IRSID PCM_RE 1108,* May 1984.

51.J.D.Seo, S.H.Kim and Kwang - Ro Lee: *Steel Research*, 69, 1998, No.2.

52.D.A.R.Kay, S.V.Subramaniyam, R.V.Kumar: *25th conference of metallurgists*, TORONTO, 1986, CIM 125-143.

53.D.Z.Lu, G.A.Irons, W.K.Lu: *Iron making & steel making*, No.2, vol.21, 1994.

54.N.A.Gokcen & J.Chipman: *AIME Trans*, 1953, vol. 197, p.173-178.

Annexure # 1

```
c       This program calculates the equilibrium metal composition
c       by using interaction parameters and equilibrium constants
c       reported by (i)Elliott and Sigworth (ii)Gaye and Gatellier
c       Slag activities are found out from iso-activity diagrams by:
c       (i)Rein and Chipman          (ii)Ohto and Suito.
c       ------------------------------------------------------------
c       "OSdata_act.in" contains slag activity by OHTO & SUITO
c       "Data_act.in" contains slag activity by REIN & CHIPMAN
c       ------------------------------------------------------------
        double precision kal2o3,ksio2,kcao,temp,ho(40)
        double precision ealal,ecaal,esial,esal,eoal
        double precision ealca,ecaca,esica,esca,eoca
        double precision ealsi,ecasi,esisi,essi,eosi
        double precision ealo,ecao,esio,eso,eoo
        double precision a,b,c,d,xnew,xold,yold,fxold,dfxold
        double precision ynew,sold,zold,znew,snew
        double precision hsi(40),hal(40),aalo(40),asio2(40),acao(40)
        double precision x1ew,y1ew,z1ew,x2ld,hca(40)
        double precision s1ew,y2ld,z2ld,s2ld
        double precision cr(40),mn(40),s(40),si(40),ca(40),o(40)
        double precision al(40)
        open(unit=22,file='OSdata_act.in')
        open(unit=23,file='Dataanal.in')
        open(unit=11,file='OS_Gaye_Result')
        write(6,*)'No. of Data Points'
        read(5,*)n
        do  k=1,n
        read(22,*)acao(k),aalo(k),asio2(k),ho(k)
        read(23,*)cr(k),mn(k),s(k),si(k),ca(k),o(k),al(k)

c       ------------------------------------------
c       Interaction Parameter by: Gaye and Gatellier
c       ------------------------------------------

        ealal = 0.044
        esial = 0.056
        ecaal = -0.072
        eoal  = -1.17
        ecal  = 0.091
        esal  = 0.03
        esisi = 0.107
        ecsi  = 0.018
        ealsi = 0.058
        ecasi = -0.097
```

```
      eosi  = -0.14
      essi  = 0.056
      ealo  = -1.98
      eoo   = -0.17
      ecao  = -310.
      esio  = -0.08
      eco   = 0.0
      eso   = 0.0
      ealca = -0.107
      ecaca = -0.002
      esica = -0.138
      eoca  = -780.
      ecca  = 0.0
      esca  = 0.0
      xold  = 10d-20

c     ----------------------
c     Equilibrium constants
c     ----------------------

      kal2o3 = 8.3333d11
      kcao   = 1111111.1
      ksio2  = 37354.60
      hal(k)=10.0**((((log10(aalo(k))))-(3.0*(log10(ho(k))))-(log1
     7 0(kal2o3)))/2.0)
      hsi(k)=10.0**((log10(asio2(k)))-(2* (log10(ho(k))))-log10(ks
     8 io2))
      hca(k)=10.0**((log10(acao(k)))-log10(ho(k))-log10(kcao))

c     ------------------
c     Initial Guess
c     ------------------

      sold=0.0
      zold=0.0
      yold=0.0

      do 200 i7=1,400
      fxold=log10(xold)-log10(hal(k))+(xold*ealal)+(zold*
     1 eoal)+(sold*esial)+(yold*ecaal)+(cr(k)*ecal)+(s(k)*esal)
      dfxold=((1.0/(2.303*xold))-ealal)
      xnew=xold-(fxold/dfxold)
            if((xnew-xold).le.1.0d-26)then
                  a=xnew
                  yold=10.0d-06
            else
```

```
                xold=xnew
            endif
200     continue

            do 300 j1=1,400
            fyold=log10(yold)-log10(hca(k))+(a*ealca)+(cr(k)*ecca
 2          )+(zold*eoca)+(yold*ecaca)+(sold*esica)+(s(k)*esca)
            dfyold=(1.0/(2.303*yold))+ecaca
            ynew=yold-(fyold/dfyold)
                if((ynew-yold).le.1.0d-09)then
                    b=ynew
                    zold=1.0d-07
                else
                    yold=ynew
                endif
300         continue

        do 400 i2=1,400
        fzold=log10(zold)-log10(ho(k))+(a*ealo)+(cr(k)*eco)
 1      +(zold*eoo)+(y*ecao)+(sold*esio)+(s(i)*eso)
        dfzold=(1.0/(2.303*zold))+eoo
        znew=zold-(fzold/dfzold)
            if((znew-zold).le.1.0d-12)then
                c=znew
            sold=0.0001
            else
                zold=znew
            endif
400     continue

            do 500 j3=1,100
            fsold=log10(sold)-log10(hsi(k))+(a*ealsi)+(cr(k)*ecsi)
 2          +(c*eosi)+(b*ecasi)+(sold*esisi)+(s(i)*essi)
            dfsold=(1.0/(2.303*sold))+esisi
            snew=sold-(fsold/dfsold)
                if((snew-sold).le.1.0d-06)then
                    d=snew
                    xold=a
                    yold=b
                    zold=c
                else
                    sold=snew
                endif
500         continue
        xlew=a
        ylew=b
```

```
      z1ew=c
      s1ew=d

      do i=1,100

      x2ld=10.0**(log10(hal(k))-(ealal*x1ew)-(ecaal*y1ew)
     1  -(eoal*z1ew)-(esial*s1ew)-(ecal*cr(k))-(esal*s(k)))
      s2ld=10.0**(log10(hsi(k))-(esisi*s1ew)-(ealsi*x2ld
     1  )-(ecasi*y1ew)-(eosi*z1ew)-(ecsi*cr(k))-(essi*s(k)))
      y2ld=10.0**(log10(hca(k))-(ecaca*y1ew)-(ealca*x2ld
     1  )-(eoca*z1ew)-(esica*s2ld)-(ecca*cr(k))-(esca*s(k)))
      z2ld=10.0**((log10(ho(k)))-(eoo*z1ew)-(ealo*x2ld)
     1  -(ecao*y2ld)-(esio*s2ld)-(eco*cr(k))-(eso*s(k)))
            if(((x1ew-x2ld).le.10d-05).and.((y1ew-y2ld)
     1      .le.10d-05).and.((s1ew-s2ld).le.10d-05).and.((z1ew-
     2  z2ld).le.10d-05))  go to 20
                  x1ew=x2ld
                  y1ew=y2ld
                  z1ew=z2ld
                  s1ew=s2ld
            enddo

 20   write(11,*)'~~~~~~~~~~~~~~~~~~~~~~~~~~~~~~~~~~~~~~~~'
      write(11,*)'h Al(slag) =',hal(k)
   write(11,*)'h Ca(slag) =',hca(k)
      write(11,*)'h Si(slag) =',hsi(k)
      write(11,*)'wt% Al   =',x2ld
      write(11,*)'wt% Ca   =',y2ld
      write(11,*)'wt% Si   =',s2ld
      write(11,*)'wt% O    =',z2ld
      write(11,*)'wt% Al(act) =',al(k)
      write(11,*)'wt% Ca(act) =',ca(k)
      write(11,*)'wt% Si(act) =',si(k)
      write(11,*)'~~~~~~~~~~~~~~~~~~~~~~~~~~~~~~~~~~~~~~~~'
c 20  write(11,*)y2ld,        s2ld,    x2ld
      enddo
      stop
      end
```